JGR Oceans

RESEARCH ARTICLE
10.1029/2023JC019915

# Shifts of the Recirculation Pathways in Central Fram Strait Drive Atlantic Intermediate Water Variability on Northeast Greenland Shelf

**R. A. McPherson[1], C. Wekerle[1], and T. Kanzow[1,2]**

[1]Alfred Wegener Institute, Helmholtz Centre for Polar and Marine Research, Bremerhaven, Germany, [2]University of Bremen, Bremen, Germany

**Key Points:**

- Warm temperature anomalies in the West Spitsbergen Current partly control Atlantic Water temperatures on the Northeast Greenland continental shelf
- Pronounced northern recirculation branches transport more Atlantic Water across Fram Strait to the northern shelf where it circulates
- Anomalous anticyclonic winds over the Barents Sea drive the enhanced recirculation of more northern Atlantic Water pathways

**Correspondence to:**

R. A. McPherson,
rebecca.mcpherson@awi.de

**Citation:**

McPherson, R. A., Wekerle, C., & Kanzow, T. (2023). Shifts of the recirculation pathways in central Fram Strait drive Atlantic intermediate water variability on Northeast Greenland shelf. *Journal of Geophysical Research: Oceans*, *128*, e2023JC019915. https://doi.org/10.1029/2023JC019915

Received 9 APR 2023
Accepted 11 SEP 2023



**Abstract** Increased oceanic heat transport plays a key role in the accelerated mass loss of Greenland's marine-terminating glaciers. The melt rate of major glaciers in Northeast Greenland (NEG) is controlled by ocean variability, in particular warm Atlantic Intermediate Water (AIW), on the continental shelf. A high-resolution configuration of the ocean sea-ice model FESOM2.1 is assessed at local and regional scales, and used to investigate the drivers of AIW temperature variability on the NEG continental shelf. The seasonal to decadal variability of AIW is characterized, featuring both pronounced interannual fluctuations and a long-term warming trend. A major source of AIW is Atlantic Water (AW) originating from the West Spitsbergen Current that recirculates in Fram Strait. AW anomalies are advected westwards and partly control the AIW temperatures on the continental shelf. Increased AIW temperatures are also connected to pronounced northern and central branches of recirculating AW in Fram Strait, and enhanced AW temperatures more regionally. The strengthening of the pathways brings more warmer AIW onto the northern part of the NEG continental shelf. There, it circulates anti-cyclonically and results in shelf-wide warming. Regional atmospheric forcing is connected to the changes in the AW circulation. The strengthening of the northern AW branches is likely caused by anticyclonic wind anomalies over the Barents Sea that drive an enhanced northward AW transport in Fram Strait. Thus, controlled by a combination of both upstream and regionally forced circulation conditions, the changes in local AIW temperatures may also affect the oceanic heat transport reaching the Central Arctic Ocean.

**Plain Language Summary** The Greenland Ice Sheet has been melting at faster rates in the last two decades, likely due to rising ocean temperatures. Warm water found below the glaciers in Northeast Greenland controls the submarine melting. Changes in the temperature of the water are connected to ocean currents on the continental shelf of Northeast Greenland and in Fram Strait. The warm water found under the glaciers originates from the West Spitsbergen Current (WSC), over several hundred kilometers away, which carries warm water northwards within the Arctic Ocean. Part of the current turns westwards and transports the warm water toward Greenland. The changes in the strength of the westward flow are connected with particular wind patterns in the Barents Sea, as the wind forcing impacts the northward transport of the warm water in the WSC. This means that more warm water flows across the continental shelf edge at higher latitudes so there is more warm water circulating on the continental shelf itself. The circulation guides this warm water through a deep channel toward the glaciers. Therefore, the variability of the water temperature below the glaciers in Northeast Greenland is controlled by both regional winds and changes in the upstream ocean currents.

## 1. Introduction

The accelerated mass loss of the Greenland Ice Sheet is one of the largest contributors to global mean sea level rise (Bamber et al., 2018; Shepherd et al., 2012). Both atmospheric and ocean warming drive the mass loss by increasing the surface and the submarine melting respectively (Kjeldsen et al., 2015; Mankoff et al., 2021; van den Broeke et al., 2009). The enhanced submarine melting, forced by oceanic heat flux, drives an increase in the ice discharge from the marine-terminating glaciers and accelerates their retreat (Holland et al., 2008; Straneo & Heimbach, 2013; Wood et al., 2021).

The oceanic heat is provided by subsurface warm water of Atlantic origin, termed Atlantic Intermediate Water (AIW), which has been found on the continental shelf of Northeast Greenland (NEG) and in a number of fjords where there are marine-terminating glaciers (Gjelstrup et al., 2022; Mouginot et al., 2015; Schaffer et al., 2017;

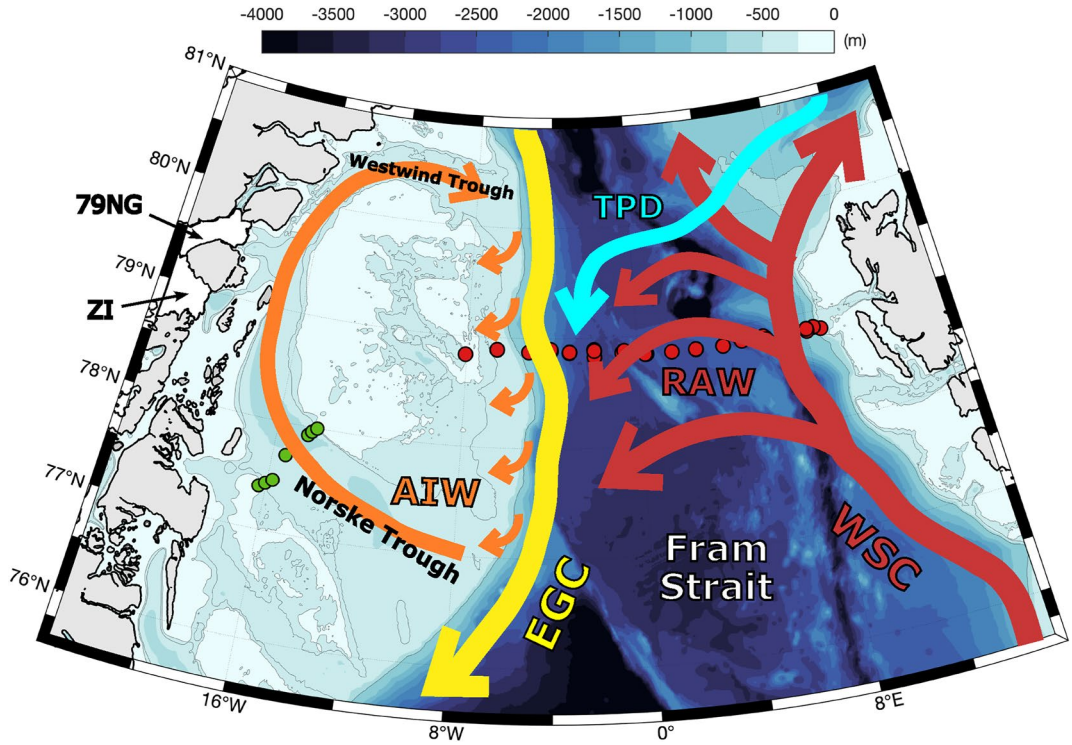


**Figure 1.** Map of Fram Strait and the Northeast Greenland (NEG) continental shelf with simplified schematic of the ocean circulation and mooring locations. Warm Atlantic Water (AW) flows northwards as the West Spitsbergen Current (WSC, red) into the Central Arctic Ocean, with multiple branches of recirculating AW (RAW) flowing westwards in Fram Strait. AW entering the Arctic Ocean is recirculated and exported as Arctic Atlantic Water (AAW). Both subsurface RAW and AAW join the East Greenland Current (EGC, yellow) which carries cold and fresh surface Polar Water (PW) exported from the Arctic along the NEG continental shelf. Freshwater outflow of PW from the Central Arctic Ocean also flows southwards in the Transpolar Drift (TPD). The Atlantic Intermediate Water (AIW, orange) which has been subducted below the PW is transported from the EGC onto the NEG continental shelf and follows an anti-cyclonic path through Norske Trough and Westwind Trough. The two main NEG glaciers are identified as Zachariae Isstrøm (ZI) and Nioghalvfjerdsfjorden (79NG). Mooring locations across Fram Strait (red) are used in Figure 4 (red) and across the Norske Trough (green) in Figure 2.

Wilson & Straneo, 2015). The AIW temperatures on the NEG continental shelf have been increasing over recent decades (Gjelstrup et al., 2022; Schaffer et al., 2017). The resultant persistent increase in the oceanic heat flux drives enhanced submarine melting of these glaciers and increased freshwater input into the ocean (Mayer et al., 2018; von Albedyll et al., 2021; Wilson et al., 2017). The two main outlet glaciers in NEG are Nioghalvfjerdsfjorden Glacier (referred to as 79 North Glacier (79NG)) and ZachariæIsstrøm (ZI), together draining over 15% of the Greenland Ice Sheet (Figure 1) (Khan et al., 2014, 2022; Mouginot et al., 2015). Recent studies have described the loss of the entire glacier tongue of ZI (Mouginot et al., 2015) and the ongoing thinning of 79NG (Mayer et al., 2018), both forced by increased submarine melting (Mayer et al., 2018; Schaffer et al., 2020; Wilson et al., 2017).

The AIW on the NEG continental shelf and below the glaciers originates in Fram Strait. Warm, Atlantic Water (AW) is carried northwards by the West Spitsbergen Current (WSC) along the eastern continental margin (Figure 1). The topographically steered boundary current has a strong seasonal cycle of mesoscale variability, with enhanced instabilities and a stronger northwards flow in winter (Tsubouchi et al., 2023; von Appen et al., 2016). The AW that flows through the Fram Strait is the dominant source of ocean heat and salt to the deep Arctic Basin (Aagaard et al., 1987; Timmermans & Marshall, 2020), and Arctic conditions are strongly influenced by changes in the properties of the AW inflow (Polyakov et al., 2017).

Approximately half of the AW flowing northwards in the WSC recirculates across Fram Strait as Recirculating Atlantic Water (RAW) and the rest reaches the Central Arctic Ocean (de Steur et al., 2014; Hattermann et al., 2016; Quadfasel et al., 1987). Observational and model studies suggest that the bulk of the circulation occurs along two main branches between 78° and 81°, separated by the Molloy Hole (Figure 1) (Hattermann

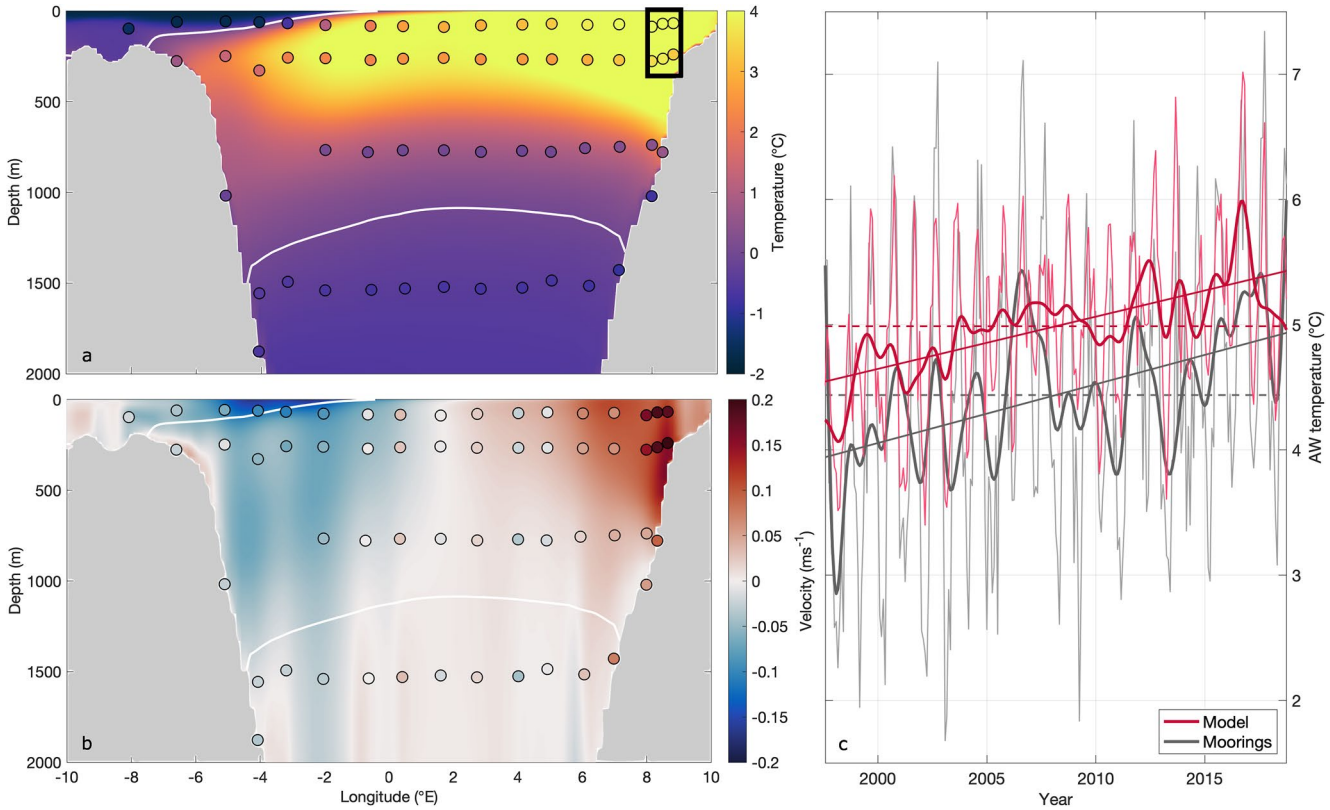


**Figure 2.** Mean longitudinal (a) potential temperature and (b) meridional velocity transect across the Fram Strait at 79°N from FESOM2.1 (filled contours). The white lines indicate the 0°C isotherms. Overlaid are average temperatures and velocities from moorings (circles). Both model and observations are averaged from Aug 1997 to Oct 2018. Positive velocities are a northward flow. The moorings correspond to those in Figure 1. Marked by the black box in (a) are the WSC moorings that are used for the (c) comparison between simulated (red) and observed (gray) AW temperatures at 75 m. Monthly means are the thin lines and a 15 months low-pass filter is the interannual signal (thick). The linear trend for both timeseries is also included in their corresponding colors, while the mean temperature for each timeseries are the dashed lines.

et al., 2016; Hofmann et al., 2021; Rudels et al., 2005; Wekerle et al., 2017). Both branches exhibit strong seasonally varying eddy activity, likely affected by the conditions set in the WSC and by the sea ice (Hattermann et al., 2016; Hofmann et al., 2021; Richter et al., 2018).

Circulating westwards, the RAW then subducts and flows southwards underneath the cold and fresh Polar Water (PW) within the East Greenland Current (EGC), which flows along the Greenland continental shelf edge (Hattermann et al., 2016; Håvik, Våge, et al., 2017; Richter et al., 2018). The EGC is also joined by returning Arctic Atlantic Water (AAW), originating from AW which enters the Central Arctic Ocean through Fram Strait and recirculates in the Eurasian and Canadian basins (Rudels et al., 2012). The shelfbreak EGC is the most prominent branch of the baroclinic boundary current, characterized by a strong near-surface-intensified southwards flow close to the NEG continental shelf edge. The AIW on the NEG continental shelf is created by the mixing of the RAW with the cold PW of Arctic origin in the EGC at the continental shelf break (Bourke et al., 1987; Schaffer et al., 2016), as well as contributions from AAW which has cooled and freshened in the Arctic Basin (Schaffer et al., 2016).

The EGC also exports sea ice through Fram Strait, accounting for approximately 90% of the total sea ice outflow from the Central Arctic (Serreze et al., 2006). This export however, has reduced in the last decades, attributed primarily to the reduction of sea ice thickness in Fram Strait which is driven mainly by atmospheric warming (Sumata et al., 2022, 2023). The shift in sea ice regime results in a strengthening of the northwards transport of AW to the Nordic Seas and Arctic Ocean (Polyakov et al., 2017; Wang et al., 2020), and is linked to changes in the atmospheric circulation (Heukamp et al., 2023; Smedsrud et al., 2022; Wang et al., 2021).

From the NEG continental shelf break, a bottom-intensified boundary current transports the AIW through the trough system on the continental shelf toward 79NG (Münchow et al., 2020). This is part of a subsurface

anticyclonic circulation of AIW on the continental shelf, where Norske Trough represents the pathway from the continental shelf edge toward the glaciers (Figure 1) (Schaffer et al., 2017). In the Norske Trough and below 79NG, AIW has large contributions of RAW whereas in the Westwind Trough, the AIW is colder and fresher as it originates predominantly from the recirculated AAW (Willcox et al., 2023). The shelf-break entrance to the Westwind Trough is located north of the main RAW branches, thus the warmer RAW does not enter through the northern inlet. A series of shallow sills in Westwind Trough act to obstruct the flow of AIW toward the inner shelf, thus this pathway plays a minor role in transporting heat toward the glaciers (Schaffer et al., 2016).

At 79NG, a sill hydraulically controls a persistent, year-round inflow of AIW into the cavity (Schaffer et al., 2020). Recent studies have shown a rapid exchange between the NEG continental shelf and the cavity at 79NG, indicating that the heat flux below the glacier is determined by the ocean conditions, namely the variability of AIW, upstream on the continental shelf (Lindeman et al., 2020; Schaffer et al., 2020; Smedsrud et al., 2022; von Albedyll et al., 2021; Wilson & Straneo, 2015). Thus understanding the processes that drive AIW variability on the NEG continental shelf are necessary to determine glacier stability.

The sustained warming of AIW on the NEG continental shelf occurs at the same time as AW temperatures in the Nordic Seas, including Fram Strait, have also been increasing (Beszczynska-Möller et al., 2012; Polyakov et al., 2017; Schauer et al., 2008). The AW temperature anomalies are advected from the WSC across Fram Strait to 79NG at a timescale of approximately 1.5 years, estimated using mean velocities from observations in Fram Strait, the EGC, and the boundary current in Norske Trough (Schaffer et al., 2017). The magnitude of warming of AIW on the NEG continental shelf is smaller than that of AW in the WSC, likely due to a combination of the colder AW subducting below the PW, atmospheric heat loss, and mixing with AAW (Schaffer et al., 2017). Longer term AIW variability (from interannual to decadal) on the NEG continental shelf appears to be connected with AW temperature variability further upstream (Smedsrud et al., 2022) though the mechanisms of the re-circulation from the WSC remain unclear. As the changing AW conditions at least partly control AIW temperatures and thus glacier retreat, it is therefore of crucial importance to determine the mechanisms and variability of the oceanic heat supply toward the glaciers.

The aim of this study is to better characterize the temporal and spatial variability of AIW temperatures on the NEG continental shelf, and determine the local and regional drivers at interannual to decadal timescales. A description of the high-resolution ocean model used for this analysis and its assessment are described in Sections 2 and 3 respectively. In Section 4, the spatial and temporal variability of AIW on the NEG continental shelf are investigated, and its links to the regional circulation in Fram Strait examined in Section 5. Finally, Section 6 discusses the local and remote drivers of AW and AIW variability in a wider context.

## 2. Model Description

In this study, we employ the Finite-volumE Sea-ice-Ocean Model (FESOM2.1) to investigate the variability of AIW properties on the NEG continental shelf and wider Fram Strait region. FESOM2.1 is a global sea-ice ocean model that solves the primitive equations under the Boussinesq approximations using the finite volume method (Danilov et al., 2017). Danilov et al. (2015) describe the sea-ice model and the global performance of FESOM2.1 is assessed by Scholz et al. (2019, 2022). Regional applications include the analysis of eddy dynamics in the Arctic Ocean (Wang et al., 2020) and heat transport into the Barents Sea (Heukamp et al., 2023).

The model is based on an unstructured triangular mesh, which enables refinement in areas of interest such as the NEG continental shelf. The triangular mesh used in this study was generated with JIGSAW-GEO (Engwirda, 2017), based on bathymetry and ice-shelf topography taken from the RTopo 2.0.4 data set (Schaffer et al., 2016). The background resolution in the global oceans was set to 1°, and refined to 25 km north of 40°N. In the Arctic Ocean including Nordic Seas, the mesh was refined to 4 km, and further refined to 2.5 km on the NEG continental shelf. Near the 79NG and ZI cavities, mesh resolution was set to 700 m. 86 vertical z-levels were used, with 5 m layer thickness in the top 100 m, and coarser layer thickness toward the ocean floor. The model setup includes an ice shelf component that resolves the cavities of the 79NG and ZI. Cavities in FESOM2.1 are treated as in the previous model version FESOM1.4, described by Timmermann et al. (2012). The interaction between ocean and ice shelf is simulated based on the three-equation system that computes salinity and temperature at the ice shelf-ocean boundary layer (Hellmer & Olbers, 1989; Holland & Jenkins, 1999). In this study, we focus on the NEG continental shelf and Fram Strait, and a detailed analysis of the cavity circulation and dynamics will follow.

In the regions with coarse resolution, isoneutral tracer diffusion (Redi, 1982) and the Gent-McWilliams (GM) Gent and Mcwilliams (1990) and Griffies (1998) eddy stirring parameterization are applied. Both GM and Redi are scaled with a horizontal resolution of a maximum value of 2,000 $m^2\ s^{-1}$ at 100 km horizontal resolution, and decreases linearly below a resolution of 40 km to reach zero at 30 km resolution. The GM parameterization is switched off when the horizontal mesh is finer than 30 km. The vertical mixing parametrization used here is the turbulent kinetic energy mixing of Gaspar et al. (1990) computed by the CVMix package (Griffies et al., 2017).

The model was forced by the JRA55-do-v1.4.0 atmospheric data set (Tsujino et al., 2018), which also includes global river runoff. For Greenland solid ice and liquid water discharge, the data sets by Mankoff, Solgaard, et al. (2020) and Mankoff, Noël, et al. (2020) respectively were used. Both data sets have daily temporal resolution and high spatial resolution (∼100 m; resolving individual streams). In the model, the surface freshwater input is treated as a virtual salt flux that is added to the salinity equation through the surface boundary condition. Sea-surface salinity was restored to the PHC 3.0 climatology (Steele et al., 2001) with a restoring velocity of $1.929 \times 10^{-6}$ $ms^{-1}$, corresponding to 50 m per 300 days.

The model run was integrated for the period 1960–2018, with a time step of 3 min. The first 10 years of the simulation are considered as spin-up, thus leaving a 49-year period for analysis with monthly mean model output.

## 3. Model Assessment

Historic hydrographic observations are used to assess the overall model performance in reproducing both the mean distribution of warm waters of Atlantic origin and their variability. The focus is both regionally in Fram Strait and more locally on the continental shelf of NEG. In this study, the warm waters of Atlantic origin are defined as AW when in the WSC with temperatures >2°C (Beszczynska-Möller et al., 2012), as RAW (>0°C) when recirculating in Fram Strait, and as AIW when below the cold (<0°C) PW surface layer, thus below the EGC, and on the NEG continental shelf. The interface between AIW and surface PW is defined by the 0°C isotherm and AIW is defined as subsurface (<150 m) and with temperatures >0°C. Mean maximum AIW temperatures are calculated by first spatially, then temporally, taking the average of the subsurface potential temperature maximum. The EGC center is located where the maximum mean southward velocities over the uppermost 150 m occur, and the boundaries where the mean velocity over the upper 150 m reduces to 20% of the core value (Håvik, Pickart, et al., 2017; Richter et al., 2018). When tracking the pathways of water of Atlantic origin across Fram Strait and on the NEG continental shelf, the AW/AIW upper boundary is defined by the isopycnal 27.7 $kgm^{-3}$, following the definition by Rudels et al. (2005) and used as an upper limit to define AW in central Fram Strait and the EGC by Hofmann et al. (2021) and Håvik, Pickart, et al. (2017) respectively.

### 3.1. Observations

Long-term mooring arrays in Fram Strait have monitored the exchange of water masses within the Arctic Ocean through the WSC (von Appen et al., 2016) and the EGC (de Steur et al., 2014) (Figure 1) On the NEG continental shelf, a mooring array across Norkse Trough observed the flow of warm AIW propagates from the continental shelf edge to the glaciers of 79NG and ZI (Münchow et al., 2020).

Additionally, the comprehensive hydrographic database of salinity and temperature for the Arctic Ocean including the Nordic Seas (UDASH, Behrendt et al. (2018)) provide a coherent spatial distribution of AIW on the NEG continental shelf. These profiles are supplemented by more recent quality-controlled data sets (OMG, 2020; Schaffer et al., 2017), resulting in over 5100 profiles on the continental shelf from 1979 to 2020. The observed hydrography and the velocity field from the moorings are used to evaluate both the mean state and variability of AW and AIW in the model simulation.

### 3.2. Fram Strait

The simulated circulation pattern in Fram Strait reproduces the inflow and outflow through distinct boundary currents. In the eastern part of Fram Strait, warm (>4°C) AW is carried northwards at mean speeds of up to 0.2 $ms^{-1}$ by the surface-intensified WSC along the Svalbard continental shelf break (Figures 2a and 2b). Toward the Greenland continental shelf on the western continental margin, the warm AW is found under a cold (<−1°C) surface layer. The western part of Fram Strait is characterized by a cold boundary current, namely the EGC, flowing southwards at speeds of up to 0.1 $ms^{-1}$.

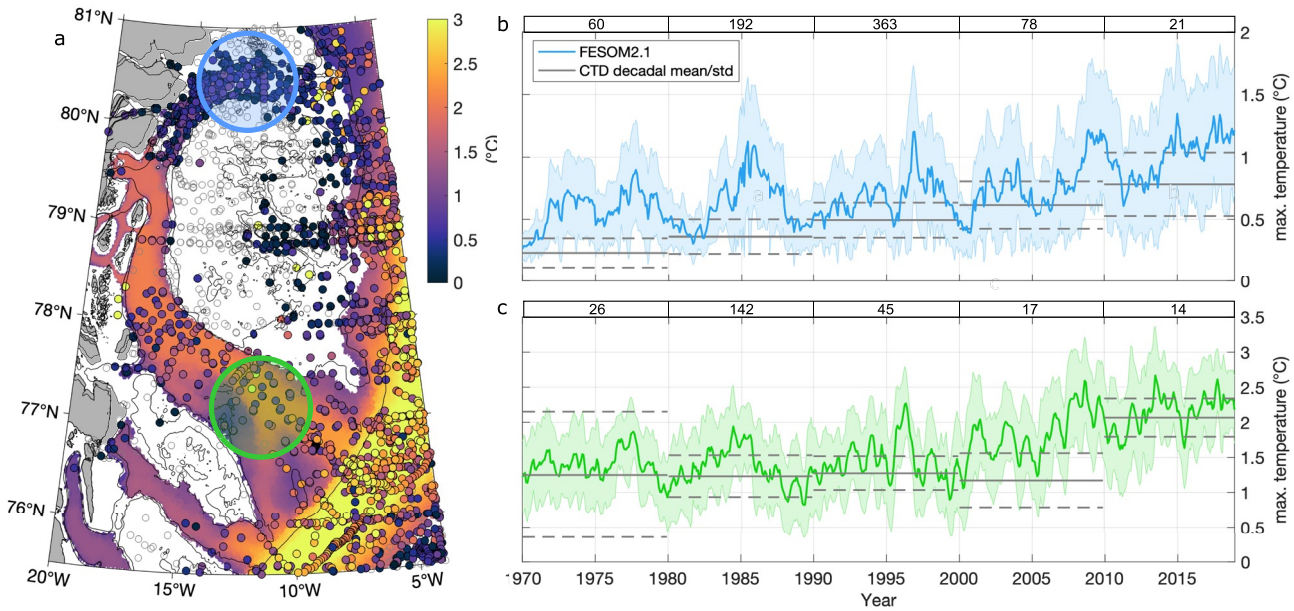


**Figure 3.** Comparison of Atlantic Intermediate Water (AIW) maximum subsurface temperature on NEG continental shelf between FESOM2.1 simulations and CTD profiles. (a) Distribution of simulated monthly-averaged maximum AIW potential temperatures with overlaid measurements from CTD profiles. The white areas correspond to where AIW was not found on the NEG continental shelf, and the gray circles represent CTD profiles in which AIW could not be identified, where AIW is defined as subsurface temperatures >0°C. The isobaths corresonding to 600, 255, 200, and 0 m are also plotted as the thin black lines. Timeseries of average maximum AIW potential temperatures in (b) Westwind Trough and (c) Norske Trough from FESOM2.1 (monthly mean) and CTD profiles (decadal mean, solid line), where the blue and green colored circles in (a) show the corresponding averaged regions in (b) and (c). The shaded area around each timeseries and the dashed lines are standard deviations of the model run and CTDs respectively. At the top of each timeseries, the number of CTD profiles used to calculate the decadal mean over the corresponding decade are noted.

The mooring observations measure the circulation pathways and thermohaline properties across Fram Strait. In the WSC, the simulated AW temperatures exhibit an interannual variability with a standard deviation of 0.6°C, and a steady long-term warming trend (Figure 2c). A linear fit reveals AW temperatures increase from 4.5°C to 5.4°C from 1997 to 2018. The observed near-surface AW temperatures display an interannual variability with a standard deviation of 0.5°C and an increase of temperatures from 4 to 5°C from 1997 to 2018. The average near-surface temperatures are 4.9°C and 4.4°C for the model and observations respectively, showing a slight warm bias in the AW temperatures by the model. This bias is recirculated westwards as simulated temperatures in the subsurface RAW (at 250 m) across the width of Fram Strait are generally 1°C warmer than the observed values (Figure 2a). Similarly, the cold PW component of the EGC, where the near-surface southward flow peaks at 4°W, has temperatures of −0.77°C and −1.5°C from the model and moorings respectively. Thus the warm bias in the model is persistent across Fram Strait.

The northward flow of AW in the WSC reaches observed speeds of 0.19 $ms^{-1}$ while simulated near-surface velocities are generally weaker, up to 0.13 $ms^{-1}$, thus underestimating the measured velocities of the eastern boundary current (Figure 2b). The EGC flows along the continental shelf break at a simulated −0.12 $ms^{-1}$ and measured −0.1 $ms^{-1}$, while the subsurface AIW, below the PW layer at 250 m, is weaker, reaching −0.05 $ms^{-1}$ in the model and −0.07 $ms^{-1}$ in the moorings. The model therefore represents the observed southward flow of the EGC and the warmer subsurface AIW below well.

### 3.3. Northeast Greenland Continental Shelf

The model simulation shows that the spatial distribution of the subsurface AIW is constrained by the bathymetry on the NEG continental shelf. Warm AIW is found along the continental shelf edge and in the deep trough system on the continental shelf, but not on the shallow plateau in the middle of the continental shelf (Figure 3a). The observations generally confirm this finding, thus the model reproduces the observed distribution of AIW on the NEG continental shelf well.

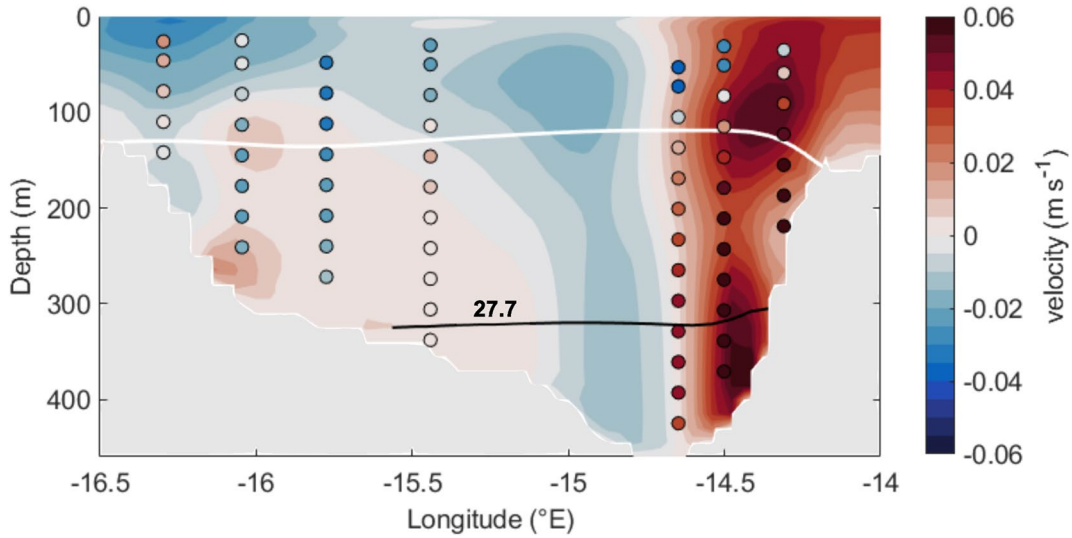


**Figure 4.** Velocity transect in Norske Trough from FESOM2.1 (filled contours) and observations superimposed (circles). The moorings were deployed from summer 2014–summer 2016 and their locations are shown in Figure 1. The simulated velocities were also averaged over the same time. Velocities are calculated perpendicular to the mooring transect; thus positive (negative) velocities are flows toward the inner shelf (shelf break). The white line represents the time-mean 0°C isotherm and the black line is the 27.7 kgm$^{-3}$ isopycnal, representing the Atlantic Intermediate Water from the model.

The simulated maximum AIW temperatures in both troughs showed high annual and interannual variability and a general warming trend. In the Westwind Trough, model temperatures steadily increase from an average of 0.63°C in the 1970s to 1.16°C after 2010 (Figure 3b). By averaging the CTD profiles over each decade, the observations also show warming from 0.20°C to 0.83°C in this northern part of the trough. Toward the mouth of Norske Trough, simulated AIW temperatures increase from 1.49°C to 2.29°C from the 1970s to after 2010 (Figure 3c). The mean CTD measurements there show a temperature increase from 1.24°C to 1.69°C. The discrepancy between the mean values in both troughs reveals a slight warm bias in the AIW temperatures across the continental shelf by the model, which is likely connected to the model's warm bias of AW in Fram Strait (Figure 2a). However, yearly model values of AIW temperatures are largely within the bounds of one standard deviation from the observed mean, thus the model generally reproduces the warming trend of AIW observed in the trough system well.

Both the observations and model results show AIW flowing through Norske Trough from the southern continental shelf edge toward the glaciers (Figure 4), a result that was well-documented by Münchow et al. (2020). This bottom-intensified jet propagates along the northern slope of the trough system. Simulated along-channel velocities reach a maximum of 0.07 ms$^{-1}$ near 350 m and reduce toward zero in the middle of the trough. Mooring records show maximum velocities of over 0.08 ms$^{-1}$ at 300 m depth, with diminishing velocities toward the channel center and above the AIW/PW interface. The model slightly underestimates the velocities of the AW flow toward the inner shelf, though reproduces the general circulation pattern of AIW through Norske Trough.

The agreement between the observations and model simulation both in the Fram Strait and on the continental shelf suggests that the model reasonably reproduces the general circulation, mean distribution, and spatial and temporal variability of Atlantic-origin waters in the region.

## 4. Atlantic Intermediate Water Variability on the Northeast Greenland Continental Shelf

In this section, the spatio-temporal variability of AIW temperatures on the NEG continental shelf are examined on interannual to decadal time scales.

### 4.1. Temporal Variability in Norske Trough

The simulated long-term mean shelf circulation pattern suggests a subsurface anticyclonic flow of AIW, where Norske Trough is the main inflow pathway for AIW from the southern continental shelf edge toward 79NG and

ZI (Figure 5a). AIW enters Norske Trough between 77 and 78°N, joining a jet-like flow moving from the continental shelf edge into the trough. This jet flows through Norske Trough toward the inner shelf at speeds of up to 0.03 $ms^{-1}$, though maximum speeds are bottom intensified and can reach over 0.05 $ms^{-1}$ (Figure 4). The AIW circulation then continues into Westwind Trough, though at reduced speeds (<0.005 $ms^{-1}$).

The spatial variability of the AIW as it flows through Norske Trough as a boundary current is examined by separating the trough into four regions. The first three are defined from the outer continental shelf edge to the inner shelf, and the fourth region is at the calving front of 79NG where the bathymetry and circulation of AIW is more complex (Figure 5a). The mean temperature profiles in each region show that a surface layer of near-freezing temperature PW (−1.8°C) overlays the warm AIW (>0°C) along the length of Norske Trough and in front of 79NG (Figure 5b). The maximum AIW temperatures decrease with distance from the shelf edge. At the outer shelf, which sets the conditions of AIW in the trough, AIW is present below 100 m, with maximum temperatures exceeding 2.2°C below 300 m. In the inner shelf, maximum temperatures of 2°C are found below 400 m. At the 79NG calving front where the water column is generally shallower, AIW peaks at 1.8°C below 300 m.

The timeseries of maximum AIW temperatures averaged over each of the four regions all display interannual variability (Figure 5c). By applying a 2–7 years bandpass-filter to each signal (not shown), the resultant standard deviation of the maximum AIW temperatures is 0.16°C at the outer shelf and 0.11°C at the inner shelf and glacier front. The temperature signals in all parts of the trough show in-phase fluctuations with little local variability, suggesting shelf-scale processes drive AIW variability. A prevalent long-term trend also shows AIW temperatures increasing throughout Norske Trough. By applying a linear fit to each timeseries, maximum AIW temperatures increase by 0.97°C at the outer shelf and 0.86°C in the inner shelf during the time period 1970–2018 (Figure 5c). However, an increase in AIW temperatures after 2000 dominates this warming trend. AIW temperatures generally increase between 0.1 and 0.2°C across the continental shelf before 2000, and rose by 0.8°C afterward. This general warming occurs at similar rates across the NEG continental shelf and at the 79NG front.

It is only at the outer shelf that a seasonal cycle is observed: a 9–15 months bandpass filter reveals a standard deviation of 0.09°C (not shown). The strength of the seasonal signal decreases with distance downstream to 0.04°C in the inner shelf and at the glacier. The maximum cross-correlation returns a time lag of 4 months in the interannual variability exists between the outer and inner shelf, and 7 months from the outer shelf to the 79NG front. This is consistent with the anticyclonic circulation observed (Figures 4 and 5a). Isolating fluctuations between 7 and 15 years reveals consistent decadal variability of 0.14°C across the continental shelf.

As there is little local spatial variability of AIW in Norske Trough (Figure 5c), with the coherent signal also extending across most of Westwind Trough (Figure 3b), a representative timeseries of AIW temporal variability is established by averaging the maximum AIW temperatures over the NEG continental shelf (Figure 5d). The focus for the remainder of this analysis is on the interannual variability of AIW properties, thus all temperature, velocity, and volume transport timeseries are filtered using a 15-month low-pass filter to eliminate annual and sub-annual oscillations. The connection between the drivers of this variability and the long-term warming trend is also examined.

### 4.2. Spatial Variability in Norske Trough

The dominant patterns of AIW interannual temperature variability on the NEG continental shelf are described with empirical orthogonal function (EOF) analysis (Figure 6). The first EOF mode resembles the spatial pattern explaining most of the variance. The corresponding principal component can then be interpreted as timeseries reflecting the temporal variability of the pattern. As a prevalent long-term trend of warming of AIW temperatures is present (Figure 5c), the EOF analysis was applied to the original and the detrended AIW temperature fields. This two-fold approach of comparing the EOFs calculated from both the original and detrended AIW temperatures examines if the trend and the interannual variability are associated with different spatial patterns.

The first EOF mode can be characterized predominantly as a pulsing shelf-wide mode (Figure 6a). This represents a warming and cooling of AIW across the whole continental shelf, showing that variability in AIW temperatures occurs shelf-wide and is not localized. The first mode explains 82% of the total variability of AIW temperatures on the NEG continental shelf. The second EOF mode captures 9% of the total variance and thus can be neglected along with higher modes (not shown).

For detrended temperatures, the first mode of variability also shows a continental shelf-wide mode associated with the AIW temperature variability (Figure 6b). This indicates that multi-annual AIW temperature changes are experienced coherently across the whole shelf. Thus, the interannual variability and long-term trend in AIW

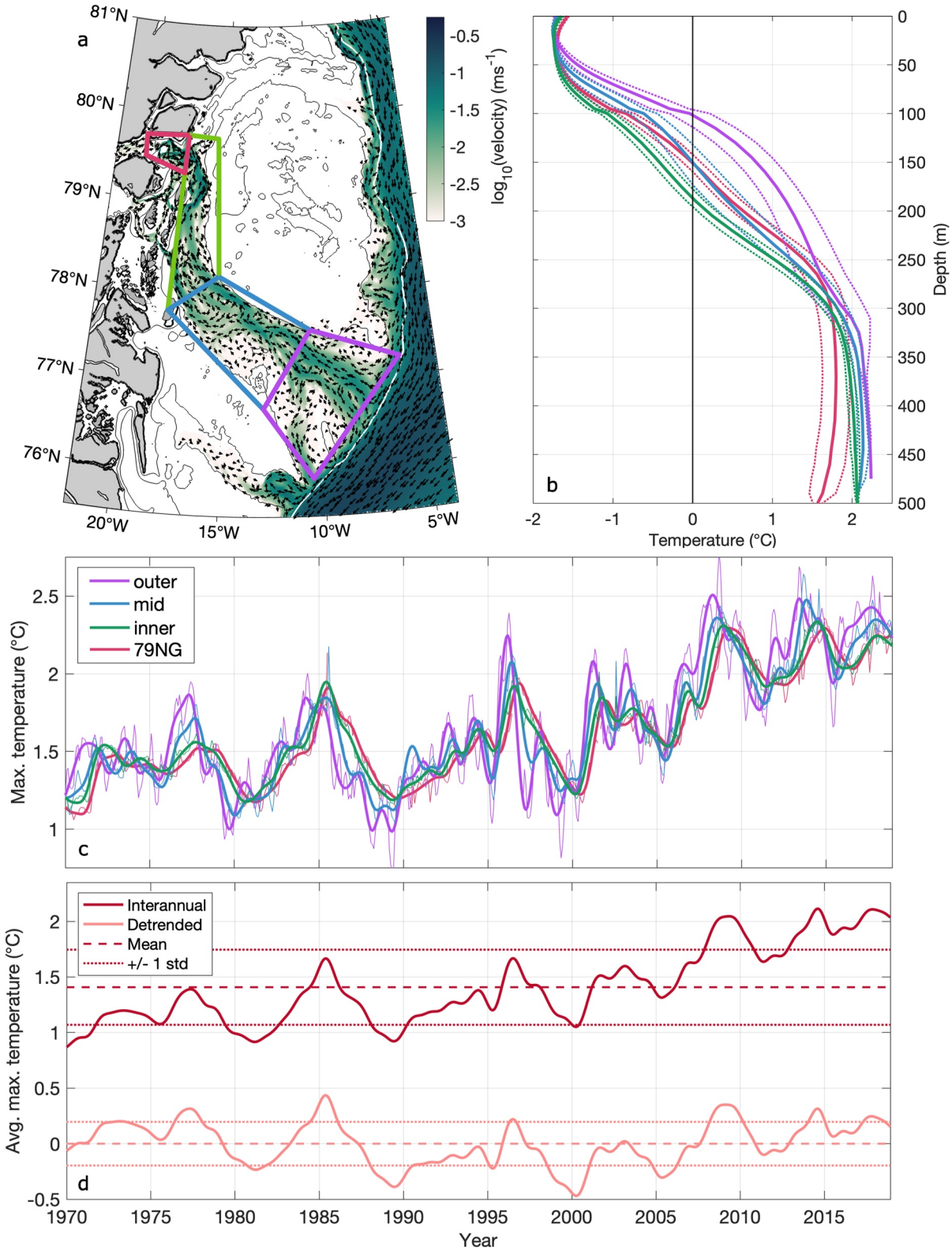


**Figure 5.**

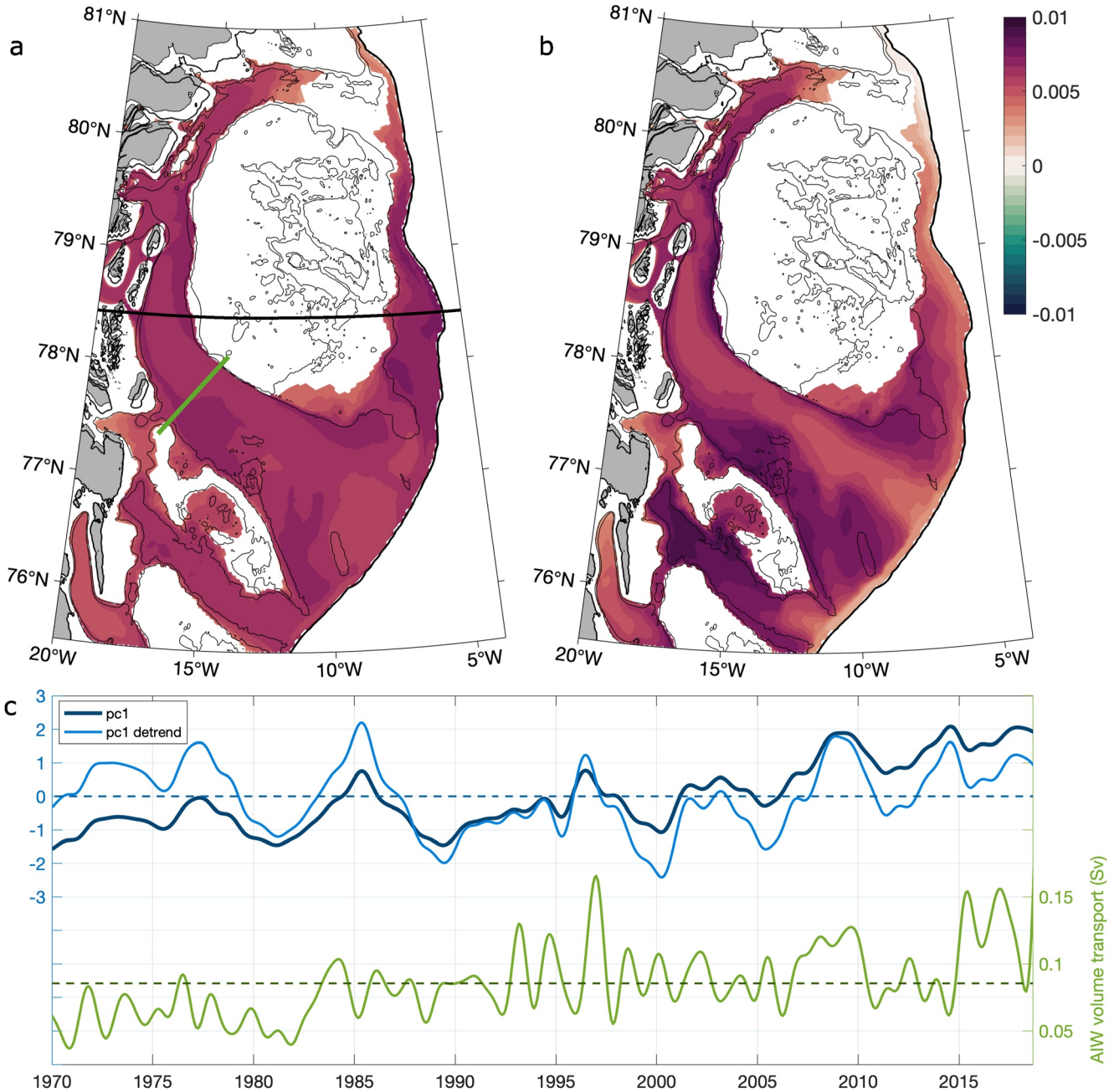


**Figure 6.** The leading EOF modes of (a) maximum Atlantic Intermediate Water (AIW) potential temperature, (b) detrended maximum AIW temperature. (c) The corresponding first principal components (blue), and the interannual AIW volume transport through the Norske Trough (green). A 15-month low-pass filter was applied to the AIW volume transport. The horizontal dashed lines are the respective mean values. Positive transport is directed toward the inner shelf, perpendicular to the transect indicated by the green line in (a). The across-shelf black line in (a) illustrates the location of the transect shown in Figure 7.

**Figure 5.** Temporal and spatial variability of simulated Atlantic Intermediate Water (AIW) temperature on the NEG continental shelf, where (a) long-term mean AIW velocities on the NEG continental shelf (color) with arrows indicating the flow direction for the time 1970–2018. The velocities are log-scaled and calculated on the 27.7 kgm$^{-3}$ isopycnal. Indicated are the four areas over which AIW properties are averaged: outer shelf (green), mid-shelf (magenta) and inner shelf (blue), and in front of 79NG (purple); (b) the average vertical temperature profiles for each area as shown in (a), with shading representing one standard deviation; (c) spatially averaged timeseries of monthly (thin) and interannual (15 months low-pass filter) (bold) maximum AIW temperature; (d) timeseries of the interannual maximum AIW temperature averaged across the NEG continental shelf (including and removing the linear trend). The dashed line is the mean value of both timeseries, and the dotted lines mark one standard deviation above and below the mean. The white line is the 600 m bathymetric contour, defining the continental shelf edge.

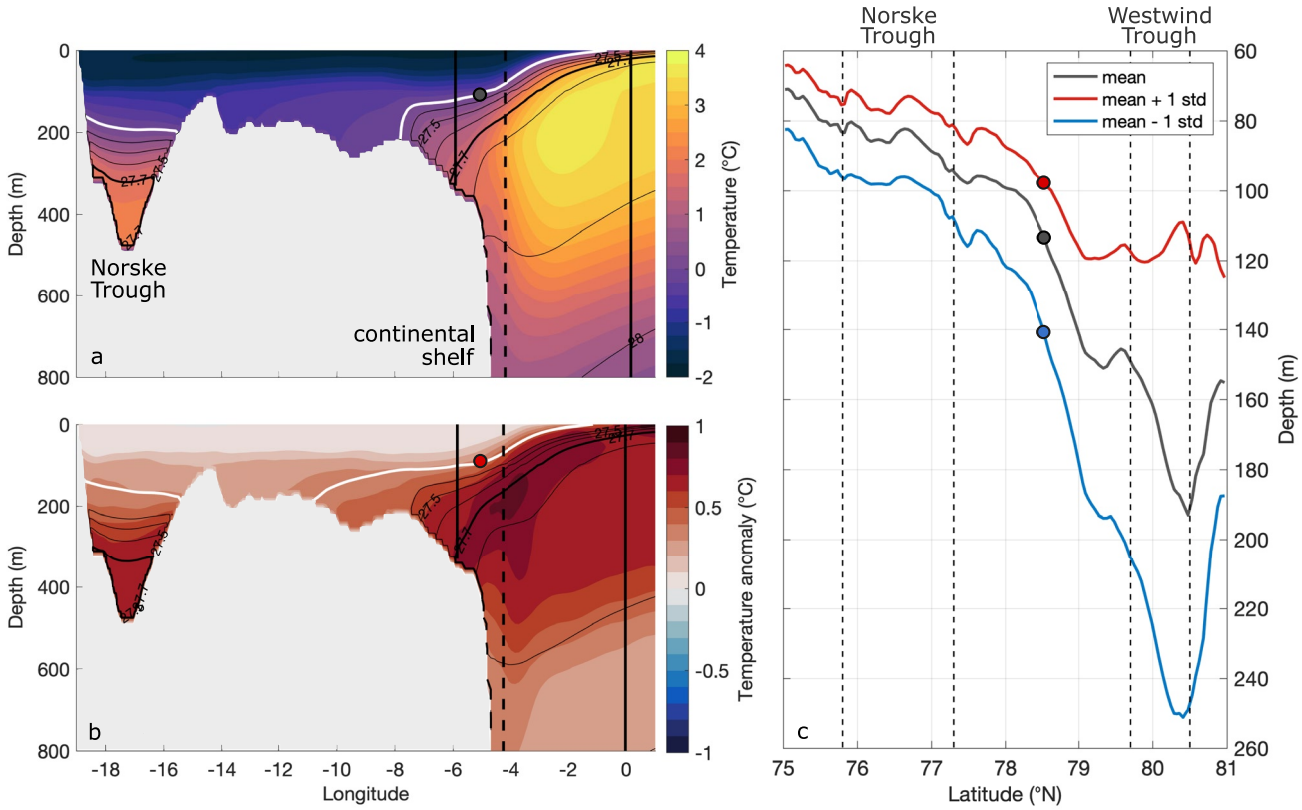


**Figure 7.** Simulated temperature across the NEG continental shelf along the 78.5°N transect (shown in Figure 6a). (a) Mean temperature and (b) composite map of temperature anomalies across the transect. Temperatures are classified as anomalous if deviating more than one standard deviation from the mean. The white lines are the 0°C isotherm for the mean temperature in each state, and the black lines are selected isopycnals. The vertical lines in (a) and (b) mark the center (dashed) and outer (solid) bounds of the EGC in each state, where the definition of the EGC is given in the text. (c) Comparison of the depth of the 0°C isotherm along the continental shelf break (600 m isobath, see Figure 5a) between 75 and 81°N and the state of anomalous warm (red) and cold (blue) Atlantic Intermediate Water temperatures. The location of the mouths of the two troughs are indicated by dashed black lines, and the isotherm depth at the transect in (a) and (b) are shown by circles for each state. The corresponding circles are also included in (a) and (b).

temperatures on the NEG continental shelf are associated with a similar spatial pattern. This first mode explains 63% of the variance and the second mode 20%.

The first principal component describes the temporal variability of the first EOF mode. The first mode for the original maximum AIW temperature timeseries displayed interannual fluctuations with a distinct pulsing (warming and cooling) of temperatures between 5 and 10 years. There is also a steady long-term increase in amplitudes over time (Figure 6c). These behaviors indicate that this first mode explains both the interannual variability and the long-term warming trend on the NEG continental shelf (Figure 6a). The first mode for the detrended temperatures displays a similar coherent cycle of interannual fluctuations between 5 and 10 years (Figure 6c), also showing a positive trend from 2000. The comparable spatial and temporal patterns between the two leading modes suggest that distinct mechanisms drive the interannual variability of the AIW temperatures on the NEG continental shelf, and are not directly connected to the long-term warming trend.

### 4.3. Connection to Volume Transport Through Norske Trough

The timeseries of AIW volume transport through Norske Trough shows that there is a persistent inflow from the southern shelf edge toward the inner shelf (Figure 6c). The volume transport exhibits an interannual variability of 0.03 Sv and has been intensifying over time. A linear trend shows an increase in 0.06 Sv between 1970 and 2018. There is a significant correlation ($r = 0.58$) between the volume transport and first principal component for the original maximum AIW temperatures timeseries (Figure 6c). After applying a 5-year low-pass filter to the transport, in order to eliminate the higher frequency signals that are not present in the first principal component, the correlation increases to 0.79. When both timeseries are detrended, the correlation decreases to $r = 0.2$ and

0.41 for the original and filtered transport respectively. This indicates a co-variability between the long-term AIW warming trend on the continental shelf and the enhanced AIW volume transport through Norkse Trough. That is, the interannual AIW temperature anomalies are at least partly connected to changes in the volume of AIW circulating on the continental shelf.

## 5. Drivers of Atlantic Intermediate Water Variability on the Northeast Greenland Continental Shelf

The drivers of the interannual AIW temperature variability on the NEG continental shelf are now investigated by compiling composite maps of temperature, velocity, sea-surface air pressure and sea-surface height during periods of anomalous AIW continental shelf temperatures. These properties have also been filtered interannually. The anomalies for the respective composite maps are calculated when the interannually-filtered average maximum AIW temperatures on the NEG continental shelf deviates more than one standard deviation from the mean (Figure 5d).

### 5.1. Link Between Atlantic Intermediate Water Variability on the Northeast Greenland Continental Shelf and East Greenland Current

An across-shelf transect from the east Greenland coast into central Fram Strait at 78.5°N shows the mean spatial distribution of AIW and the EGC (Figure 7a). A relatively quiescent surface layer of cold (<0°C) PW sits above the NEG continental shelf and extends into Fram Strait. In Norske Trough, warm AIW is present below 200 m, reaching temperatures of up to 2°C. On the continental shelf, AIW is not found on the shallow plateau; instead, AIW sits on the shelf edge below 200 m at ∼8°W. Offshore, warm RAW is present at the surface in central Fram Strait and then below the PW layer closer to the continental slope (Figure 7a). The highest temperatures exceeding 4°C are found at 200 m, below the PW in the offshore side of the EGC. The location of the core of the EGC, centered at 4.2°W, occurs at the hydrographic front of AIW and PW, where the 27.7 $kgm^{-3}$ isopycnal shoals steeply. The EGC extends from the NEG continental shelf break at 6°W into central Fram Strait, approximately 140 km in width. This is wider than estimates made from velocity observations by Håvik, Pickart, et al. (2017) which found a maximum EGC width of 80 km, though further south below Norske Trough. As the EGC generally decreases in width as it propagates south through Fram Strait, a wider core upstream at 78.5°N (Figure 6) is not unexpected.

Periods of positive AIW temperature anomalies on the NEG continental shelf coincide with a general increase in AIW temperatures in the EGC (Figure 7b). In the Norske Trough, this is equivalent to a warming of over 0.5°C. At the center of the EGC, at the continental shelf edge, a concentrated core of positive AW temperature anomalies of almost 1°C is found below the PW layer. The temperature anomalies offshore decrease with depth. There is no temperature change in near-surface PW above 100 m. Overall, however, the position of the EGC near the shelf break and its width show only minor changes between the mean and anomalous state (Figures 7a and 7b), equivalent to a slight narrowing of the boundary current by 6 km about a stable core position.

Associated with the positive anomalous AIW temperatures is also a westward shift in the location and distribution of the AIW on the continental shelf itself. From its mean state at the shelf break, the AIW/PW interface, defined as the 0°C isotherm, moves to the middle of the shallow plateau at 11.5°W (Figures 7a and 7b). The shift corresponds to a westward migration of over 65 km. The layer of AIW in Norske Trough also thickened by almost 50 m, suggesting the resultant increase in the volume of AIW on the eastern part of the continental shelf circulates through the trough.

The shoaling AIW is observed along the length of the continental shelf break. The depth of the 0°C isotherm along the 600 m isobath shows a general thickening of the AIW layer connected to the positive AIW temperature anomalies (Figure 7). The greatest shoaling of the 0°C isotherm occurs at the northern end of the continental shelf, in Westwind Trough, rising from 180 to 120 m. The difference in layer thickness decreases toward Norske Trough, with changes of less than 10 m near the southern end of the shelf. As this coincides with the general warming of AIW across the continental shelf (Figure 7b), it means that more and warmer subsurface AIW is present on the eastern side of the NEG continental shelf, with the dominant increase in AIW volume at higher latitudes (Figure 7c). The AIW then circulates on the continental shelf, consistent with the relationship found between the AIW volume transport and temperatures on the continental shelf (Figure 6d).

The spatio-temporal variability of AIW temperatures on the NEG continental shelf have been characterized here. The interannual variability coincides with a westward migration of AIW from below the EGC onto the continental shelf itself. In order to determine the forcing mechanisms of this lateral shift, the connection between the interannual AIW temperature variability and upstream conditions is now investigated.

### 5.2. Shifting Recirculation Pathways of Atlantic Water in Fram Strait

Warm and salty AW originating from the WSC partly recirculate in Fram Strait and supplements the southward flow of the EGC (Figure 1). Thus, variability in the WSC could be advected westwards and control AIW temperatures on the NEG continental shelf. The role of advection in controlling temperature anomalies on the NEG continental shelf, originating in the WSC, can be examined by comparing temperature timeseries in both locations.

A linear fit applied to the simulated AW temperatures in the WSC between 1970 and 2018 (Figure 2c) revealed a general warming rate of 0.35°C/decade. The observations show an increase of 0.5°C/decade between 1997 and 2018, while the model presents a 0.44°C/decade warming rate over the equivalent time. On the NEG continental shelf (Figure 5d), AIW temperatures were generally lower than in the WSC by an average of 3°C due to a likely combination of heat loss to the atmosphere (prior to subduction) (Hattermann et al., 2016), the subduction of the colder component of the AW, and subsequent mixing with the cold PW. By applying a linear fit to the AIW temperatures before and after 2000, the AIW warming rates increase from 0.08°C/decade by more than a factor of five to 0.41°C/decade. Schaffer et al. (2017) compared maximum AIW temperatures from CTD profiles in Norske Trough between 1979 - 1999 and 2000–2016, and found an average increase of 0.5°C. Averaging the simulated AIW timeseries (Figure 5d) over the same time ranges reveals a warming of 0.45°C.

The maximum temperatures at the two locations on either side of Fram Strait are positively correlated with a statistically significant maximum value of $r = 0.8$ at a lag of 21 months. When the long-term trend of both timeseries is removed, the maximum correlation value decreases to $r = 0.5$. This suggests that the interannual variability of AIW temperatures is at least partly explainable by an advection of AW temperature fluctuations from the WSC via the recirculation branches across Fram Strait. Yet, a correlation of 0.5 leaves a sizable fraction of interannual AIW variability on the continental shelf unaccounted for by simple advection at a constant velocity.

The positive NEG AIW temperature anomalies are also associated with a general warming of AW across the whole Fram Strait (and cooling during negative anomalies) (not shown). There is an increase in AW temperatures of 0.5°C in the WSC and between 0.5 and 1°C in the RAW found in central Fram Strait. These positive temperature anomalies result in the AIW component of the EGC warming by 0.8°C.

In the following, we investigate whether circulation changes may also affect the connection of AIW temperature between the WSC and the NEG continental shelf. For this, the mean AW circulation in Fram Strait is determined by averaging the AW velocity components on the 27.7 $kgm^{-3}$ isopycnal; a representative density of AW/AIW across Fram Strait (Figures 4 and 7a). The mean circulation pattern reveals the strong exchange flow of AW through Fram Strait, and the various RAW pathways that connect them (Figure 8a). Specifically, the vector fields show three distinct branches of westwards flow in the central Fram Strait. Between 5 and 1° E, AW flows northwards in two distinct branches. Following the continental slope of Svalbard, the onshore component of the WSC transports AW north at speeds exceeding 0.2 $ms^{-1}$, while a slower branch is found offshore. The onshore WSC bifurcates at 79°N: a part continues northwards along the Svalbard continental shelf edge while the rest turns westwards and further splits into two pathways. A larger, more central branch (middle branch) turns westwards at around 79°N with average speeds of 0.06 $ms^{-1}$, and a second, weaker, pathway (northern branch) recirculates further north at 80°N. The offshore WSC recirculates across Fram Strait at 78°N as a southern branch, reaching speeds of over 0.1 $ms^{-1}$.

All three branches of RAW join the southward flow along the Greenland continental shelf break. The RAW branches meet the subsurface AAW, exported from the Central Arctic Ocean, at 78.5°N, and the southern branch forms an offshore branch of the EGC at 78°N. The AIW within the EGC is carried southwards along the continental shelf edge at speeds of over 0.2 $ms^{-1}$. The presence and location of multiple recirculation branches agrees with previous studies that have observed the circulation structure of RAW in Fram Strait (Hattermann et al., 2016; Hofmann et al., 2021), though their location and extent are further discussed in Section 6.2.

In order to detect the role of the circulation in Fram Strait for the AIW temperatures on the continental shelf, composite maps of the velocity anomalies are compiled. To focus on the upstream recirculation pathways, a

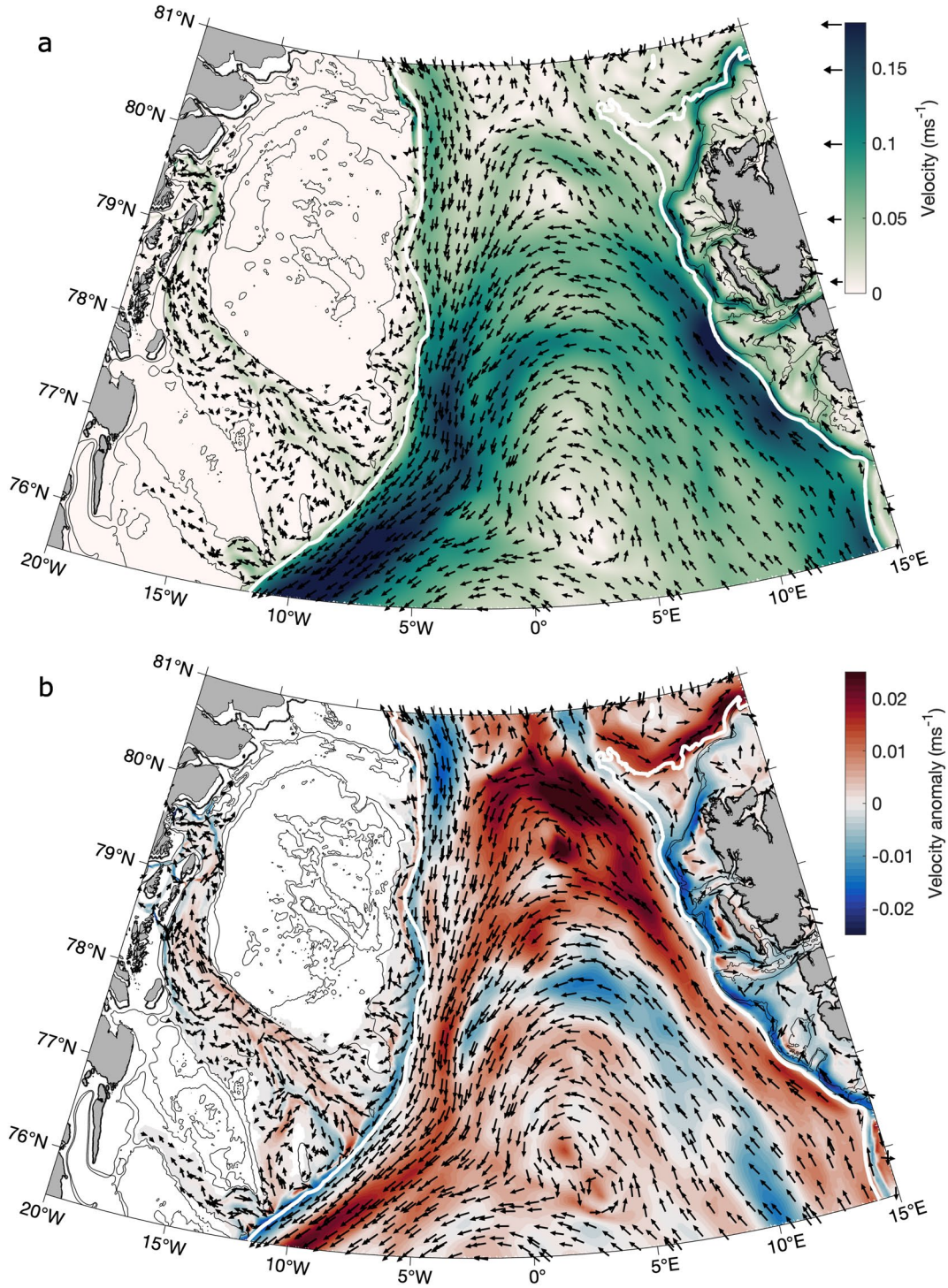


**Figure 8.** AW circulation pathways in Fram Strait associated with positive Atlantic Intermediate Water (AIW) temperature anomalies. (a) Mean velocity and (b) time-shifted composite map of velocity anomalies of AW in Fram Strait. AW is defined as the properties on the 27.7 kgm$^{-3}$ isopycnal. The mean circulation pattern (arrows) are drawn with a logarithmic scale for each state, and included on the colorbar for scale. The composite map is calculated by averaging the velocity anomalies (i.e., time mean subtracted) during time periods shifted by 19 months backwards in time relative to when the maximum AIW temperatures on the NEG continental shelf exceed the temporal mean by one standard deviation. The red color represents a strengthening of the flow, and blue is weakening. The white lines are the 600 m bathymetric contours, indicating the continental shelf edge.

backward shift of 19 months is applied to the times when there are positive AIW temperature anomalies on the continental shelf (Figure 5d). This considers the 21-month lag between the interannual temperature fluctuations in the WSC and on the NEG continental shelf and the advective time scale of 1–2 months for temperature anomalies to arrive in the western part of Fram Strait (von Appen et al., 2016; Hattermann et al., 2016). The AW velocity anomaly components are averaged over these backwards shifted times. Though this lag does not fully represent the corresponding AIW response in the EGC, which requires a further 2 months to reach Norske Trough (Schaffer et al., 2017), applying a lag of 17 months reveals a similar pattern (not shown). The analysis reveals a coherent, regional pattern of the AW circulation pathways in Fram Strait associated with positive AIW temperature anomalies on the NEG continental shelf (Figure 8b) as follows. Both boundary currents—the WSC and the EGC—exhibit changes in flow speeds. The onshore component of the WSC shows a strengthening of the northward flow, with positive velocity anomalies reaching 0.015 $ms^{-1}$, while the offshore branch weakens by up to 0.01 $ms^{-1}$. At the same time, the sensitivity of the shelfbreak EGC can be expressed as a two-branch response. The narrow onshore branch shows a distinct northward velocity anomaly, illustrating a weakening of the EGC along the length of the continental shelf break, while the offshore branch of the shelfbreak EGC, composed predominantly of the recirculated northern and middle RAW branches, generally accelerates its southward flow.

The three RAW branches also show significant velocity anomalies, connected to the change in the boundary currents that feed them (Figure 8b). The southern recirculation branch at 78°N, fed by the weakened offshore branch of the WSC, exhibits a decrease in the mean westward velocity of approximately 25%. The two more northern pathways, fed by the strengthened onshore WSC, display positive westward velocity anomalies, which corresponds to an increase in speed of the recirculation branches. The middle branch at 79°N increases in speed by 0.01 $ms^{-1}$, the equivalent of 15% relative to its mean flow, and the northern branch by over 40%. It is re-assuring that a similar pattern is found to that in Figure 8b for the composite velocity pattern using the linearly detrended AIW case (not shown). The distinct changes in the patterns of AW circulation in Fram Strait indicate that AIW temperature variability on the NEG continental shelf is connected to mechanisms which control the recirculation pathways.

The changes in the strengths of the different recirculation branches may in part result from regional wind patterns. In order to establish any consistent wind patterns associated with anomalous AIW temperatures on the NEG continental shelf, the composites are extended to sea level pressure (SLP). A 19-month backward time shift is again applied to the composites to account for the transit time for AW to reach and circulate on the NEG continental shelf. The pattern of SLP in the wider region around Fram Strait associated with high anomalous AIW temperatures on the NEG continental shelf correspond to an anomaly with a high-pressure center to the east of Svalbard in the Barents Sea and low-pressure in central Fram Strait extending south into the Greenland Sea (Figure 9a). The distribution of the SLP anomaly results in an anti-cyclonic atmospheric circulation anomaly in the north near Svalbard and into central Fram Strait. The gradients then drive a generally northward wind anomaly through Fram Strait which strengthens the northward flow of the WSC (Figure 8b) by causing an eastward Ekman transport along the continental slope of Svalbard.

Anomalous SLP gradients peak over Svalbard and weaken westward toward Greenland and again toward the Greenland Sea in the south. This would be roughly consistent with a decrease in sea-surface height (SSH) in central Fram Strait, as the Ekman transport pushes the water toward the Svalbard shelf where it converges. Indeed, the actual composite map of SSH (corresponding to positive AIW anomalies on the NEG continental shelf with a 19-month time lag) reveals positive SSH anomalies in northern Fram Strait and on the Greenland and Svalbard continental shelves (Figure 9b). In central Fram Strait, negative SSH anomalies are generally found, with a distinct region of negative SSH anomalies between 79 and 81°N—where the middle and northern branches of RAW circulate (Figure 8). The pronounced SSH gradient through central Fram Strait sets up an anomalous northward geostrophic flow in northeastern Fram Strait, which acts to strengthen the RAW pathways farther north. North of Svalbard, in the absence of an eastern boundary, this anomalous transport feeds the northern recirculation branch.

## 6. Discussion

### 6.1. West Spitsbergen Current

The results presented here show that the interannual AIW temperature anomalies on the NEG continental shelf are partly controlled by the mean advection of AW temperature anomalies from the WSC across Fram Strait. Thus, the temperature variability in the WSC (Figure 2c) ultimately sets the boundary conditions for AIW variability on

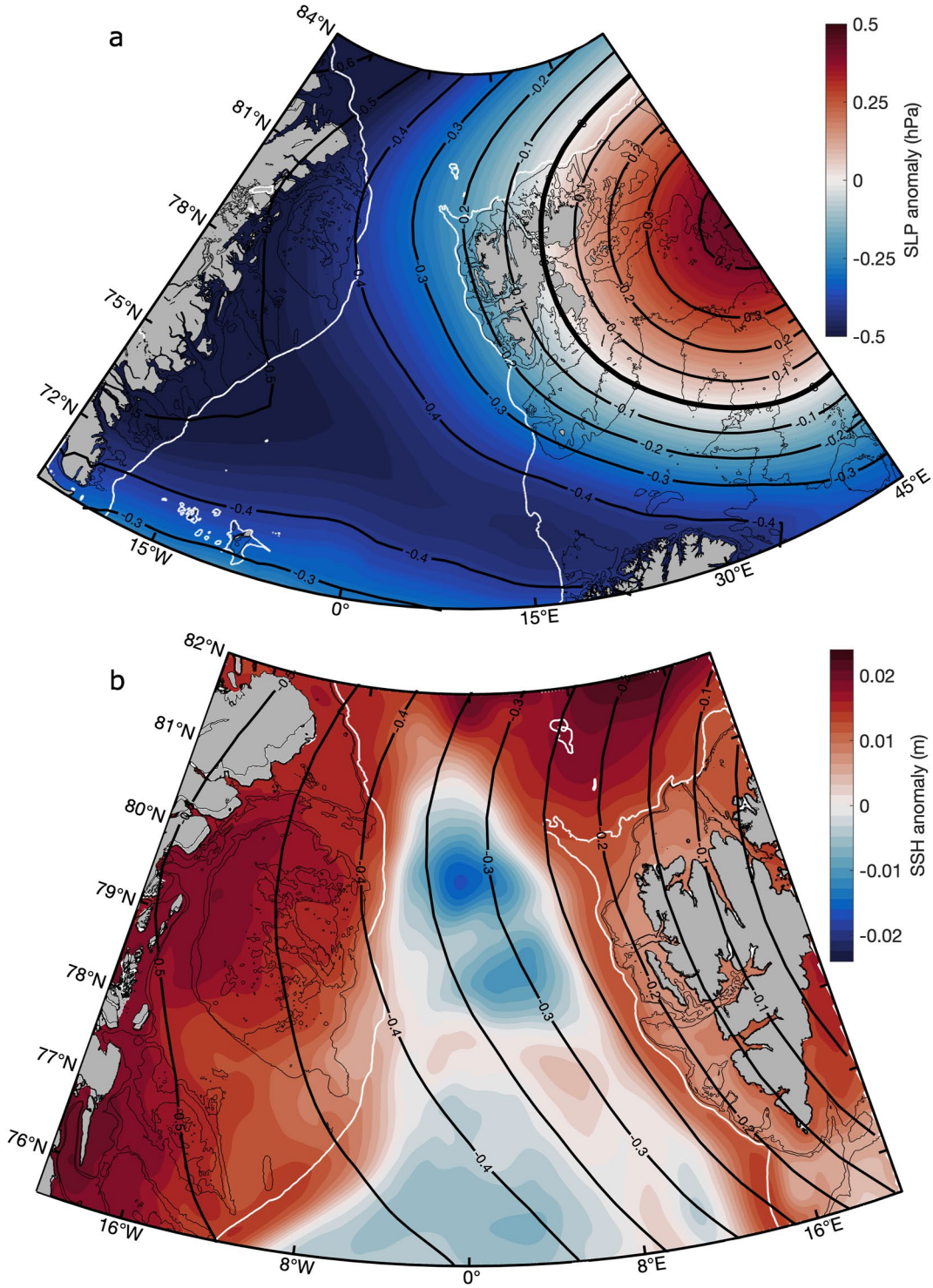


**Figure 9.** Composite map of the anomalous (a) sea level pressure (SLP) anomaly over the wider Fram Strait and Barents Sea region, and (b) sea-surface height (SSH) in central Fram Strait. The composite maps are calculated by averaging the SLP and SSH anomalies when the maximum Atlantic Intermediate Water temperatures (with trend) on the NEG continental shelf exceed the time mean by one standard deviation, shifted backwards by a 19-month lag period. In both panels, positive anomalies are red and negative anomalies are blue, and the contour lines are SLP anomalies at intervals of 0.1 hPa (a) and 0.05 hPa (b). In (a), the 0 hPa contour line over Svalbard is marked in bold. The white lines indicate the shelf break.

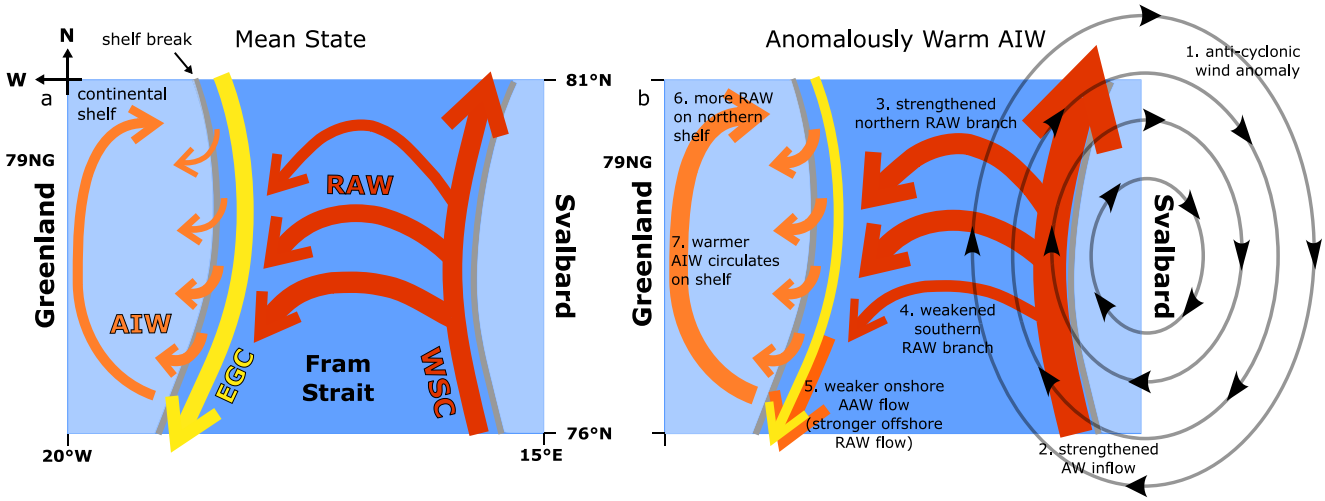


**Figure 10.** Schematic of the proposed mechanisms that determine the Atlantic Water circulation pathways in Fram Strait. (a) Mean and (b) anomalous circulation of AW when Atlantic Intermediate Water (AIW) temperatures on the NEG continental shelf are high. The inverse case is true for negative AIW temperature anomalies. In (b), the thicker (thinner) arrows mean stronger (weaker) flow relative to the mean state in (a). The numbering refers to the order in which the processes are connected and are explained in the text. The abbreviations are also defined in the text.

the NEG continental shelf. In addition, regional wind forcing in the eastern Fram Strait affects both the strength and spatial structure of the WSC at interannual timescales. An anti-cyclonic atmospheric circulation pattern over Svalbard and central Fram Strait (Figure 9a) sets up SSH gradients (Figure 9b) which strengthen the northward flow of the boundary current (Figures 8b and 10). Previous studies have also shown that wind-driven forcing in the Nordic Seas drives variability in the northward flow of AW by the same mechanisms, namely that atmospheric forcing drives Ekman transport which leads to SSH gradients and changes in the geostrophic flow (Chafik et al., 2015; Heukamp et al., 2023; Muilwijk et al., 2018, 2019). At interannual timescales, Chafik et al. (2015) find that wind anomalies over Svalbard and the northern Barents Sea, connected to positive SLP anomalies over the area, set up Ekman transport. This promotes a positive SSH gradient toward Svalbard and thus enhances northward AW transport in the WSC at interannual scales. At decadal timescales, the AW volume transport in the WSC through Fram Strait is highly correlated with the wind stress curl in the Nordic Seas (Muilwijk et al., 2018). As increases in AW volume transport correspond to an increase in the northward heat transport of the WSC (Schauer, 2004), this suggests that the strengthening of the WSC by upstream wind conditions increases the heat transport through Fram Strait.

The AW temperatures in the WSC are also generally characterized as having a pronounced seasonal cycle (Figure 2c). Studies have characterized the seasonal variability in the AW temperature and volume transport of the WSC (Beszczynska-Möller et al., 2012; Schauer, 2004; Tsubouchi et al., 2023; von Appen et al., 2016; Wekerle et al., 2017). In winter, the AW is impacted by pronounced atmospheric cooling over the Nordic Seas, which weakens the near-surface stratification (Boyd & D'Asaro, 1994). There is also stronger wind stress over the Nordic Seas in winter (Jakobsen, 2003) which strengthens the cyclonic Greenland Sea Gyre circulation (Chatterjee et al., 2018). These factors combine to promote a stronger northward flow of the WSC in winter months. The strengthening of the WSC also implies the boundary current is less stable; thus the enhanced baroclinic instability leads to increased eddy kinetic energy in the WSC compared to summer months (von Appen et al., 2016). The eddies are then advected westwards (Hattermann et al., 2016; von Appen et al., 2016; Wekerle et al., 2020), meaning that the stronger eddy fluxes in the WSC in winter promote a stronger recirculation and thus a larger heat flux into the AW recirculation. It is currently an open question how eddies modulate the extraction of heat from the WSC into the AW recirculation branches on interannual to decadal time scales, which are considered in our study.

### 6.2. Recirculation Branches

In addition to temperature anomalies in the WSC, the AIW temperature anomalies on the NEG continental shelf are linked to changes in the strength of the recirculation branches of AW across Fram Strait (Figure 8).

When NEG continental shelf AIW temperatures are high, the middle and northern branches of RAW are more pronounced while the southern branch weakens (Figures 8b and 10). The AW temperatures in the WSC are also simultaneously higher at these times, thus more and warmer RAW is advected westwards at higher latitudes. The onshore branch of the WSC feeds the middle and northern RAW pathways (Figure 8a), which have been previously observed in high-resolution models and moored observations (Hofmann et al., 2021; Quadfasel et al., 1987; Richter et al., 2018; Wekerle et al., 2017). The middle branch is present year-round as a mean flow, while the northern branch is strongly seasonal, disappearing entirely in summer (Hofmann et al., 2021; Wekerle et al., 2017). Hofmann et al. (2021) described the seasonal variability of both branches. They showed a time lag of a few months existing between the peak eddy kinetic energy in the recirculation branches and in the WSC, indicating that the RAW properties originate in the WSC and are advected by the mean flow of the recirculation branch. The proportion of AW that recirculates in Fram Strait and that enters the Central Arctic Ocean directly is also seasonal (de Steur et al., 2014; Rudels, 1987). Hattermann et al. (2016) revealed that up to 60% of AW recirculates in late winter/spring and 30% recirculation occurs in summer. It is speculated that the intensification of the RAW branches in winter months is linked to the enhanced eddy activity in the WSC (Hattermann et al., 2016; Wekerle et al., 2017).

The offshore branch of the WSC feeds the southern recirculation branch (Figure 8a) (de Steur et al., 2009, 2014). The AW in this branch originates primarily from the Norwegian Atlantic Front Current and is composed of AW and the cold and saline Arctic Ocean Deep Water (Hattermann et al., 2016). The AW in the offshore branch is colder and fresher than in the onshore WSC. The observed weakening of the recirculating southern branch associated with a positive SLP anomaly around Svalbard (Figure 8b) indicates a reduction of the colder AW that recirculates in southern Fram Strait. However, as the southern branch forms the offshore component of the EGC (Figure 8a), its change will likely only affect the AIW temperatures on the NEG continental shelf in a minor way.

Regional wind forcing is not only the driver of changes in the WSC but also affects the strength and structure of the downstream RAW branches. An anticyclonic atmospheric circulation anomaly over Svalbard strengthens the WSC (Figure 8b). This increase in northward flow is then circulated westwards by the northern and middle branches (Figures 8b and 10). The corresponding anomalous SSH gradients in central Fram Strait represents a northerly migration in the circulation branches, which causes more RAW to recirculate at higher latitudes. These results bear strong similarities to those obtained by Heukamp et al. (2023). Using an ocean-sea-ice model, they found that wind anomalies near Svalbard significantly impacted the AW recirculation in Fram Strait. In their model study, an anomalous cyclonic wind forcing was imposed in the Barents Sea, associated with multi-decadal sea-ice retreat in northern Barents Sea, and a corresponding southwards migration of the recirculation pathways was found. Mechanically, the southwards component of the wind anomaly over Svalbard shifts the WSC westwards, down the continental shelf, and causes an increase in the SSH in central Fram Strait which extends up to 80°N. They argued that the offshore migration of the WSC then reduces the amount of AW reaching the more northern recirculation pathways, and instead causes the AW to recirculate at lower latitudes. As a result, AIW temperatures on the NEG continental shelf were generally lower compared to a control experiment (F. Heukamp et al., 2023, personal communication). The wind stress curl can also explain the temporal variability of the southern circulation branch (de Steur et al., 2014) as it is composed of AW from the wind-driven cyclonic gyre in the Nordic Seas. Anomalous wind stress therefore modifies its strength by inducing SSH anomalies which affect the circulation pattern (Chatterjee et al., 2018), and in turn the southern branch. Therefore, it is proposed that the regional wind forcing not only promotes variability in the WSC that is advected westwards, but also affects the strength and behavior of RAW pathways through which all AIW passes. Heukamp et al. (2023) also found that because more AW was transported westwards along more southerly pathways, less heat entered the Central Arctic Ocean. This suggests that both the AW temperature anomalies in the WSC and the behavior of the recirculation pathways by which AW is advected across Fram Strait ultimately controls the AIW on the NEG continental shelf. It also implies that the regional atmospheric circulation can directly impact the heat that enters the Arctic Basin through Fram Strait.

### 6.3. East Greenland Current

All three of the recirculation branches join the southwards flowing EGC along the Greenland continental shelf (Figure 8a), and their variability affects the boundary current. The pronounced northern and middle RAW pathways lead to enhanced southwards velocities (Figure 8b) and increased AIW temperatures (Figure 7b) in the

offshore branch of the EGC into which they feed. The enhanced westward flow also brings more and warmer AIW to the NEG continental shelf at higher latitudes (Figure 10). The increase in thickness of the AIW layer along the NEG continental shelf break north of 79°N (Figure 7c) illustrates clearly that the AW from the RAW branches reaches the more northern parts of the NEG continental shelf edge and moves further westwards onto the continental shelf (Figures 7a and 7b). At the same time, the southwards flow of the colder AAW exported in the onshore branch EGC along the continental shelf edge is reduced (Figures 8b and 10).

However, the change in flow conditions does not correspond to an onshore migration or broadening of the velocity field of the EGC itself (Figures 7a and 7b). Other processes must then transport AIW from the EGC and across the NEG continental shelf edge. Håvik and Våge (2018) suggested that episodic wind-driven upwelling leads to across-shelf currents that lift warm AIW onto the NEG continental shelf. However, they also found that the region of most upwelling-favorable wind conditions tends to occur further south; that is, south of 72°N, near Denmark Strait. In the case of our study region in contrast to those areas further south along the EGC, the offshore subsurface core of AIW is located at depths shallower than the depth of the continental shelf break (Figure 7a). Therefore, simple lateral eddy mixing is sufficient to flux AIW onto the continental shelf of NEG, especially during times of a strengthened northern recirculation branch when the upper AIW boundary is displaced upwards by up to 60 m compared to mean conditions (Figure 7c). In support of this statement, Schaffer et al. (2017) hypothesized that AIW in the EGC may be transported onto the continental shelf via eddy- and tidally driven mixing, and eddy overturning has been observed to play an important role in cross-shelf exchanges in Fram Strait (Tverberg & Nost, 2009) and elsewhere (Cherian & Brink, 2018). The substantial mesoscale activity in the AIW layer of the EGC (Håvik, Våge, et al., 2017) supports this theory. Münchow et al. (2020) showed that strong winds acting over the steep slope of the continental shelf edge near the mouth of Norske Trough would generate topographic Rossby waves from the Ekman pumping. These baroclinic waves would then propagate across the continental shelf and into the trough system, and might be associated with additional cross-shelf edge heat fluxes. This, however, is a phenomenon that acts at weekly to monthly time scales. It is unclear, if it is also relevant on interannual time scales. While it remains unclear which processes drive the across-shelf flow, the interannual signals in the WSC that are carried westwards and join the EGC before reaching the NEG continental shelf, are well preserved during the cross shelf-edge exchange.

### 6.4. Northeast Greenland Continental Shelf

The AIW anomalies are driven from the EGC across the NEG continental shelf break and circulate through the trough system. The weak local variability of the AIW temperature signals over the length of Norske Trough and their lagged response (Figure 5c) implies that the interannual variability originates from the outer shelf and AIW is advected by the bottom-intensified boundary current toward the inner shelf and 79NG (Figure 4). A dominant monopole-like first EOF mode shows that interannual AIW temperature changes occur through the whole trough system (Figure 6a), indicating a shelf-wide circulation of AIW. The westward shift of AIW across the continental shelf break (Figures 7a and 7b) increases the volume of the AIW that enters into the anti-cyclonic circulation from the continental shelf edge (Figure 5a) and ultimately propagates through Norske Trough (Figures 6d and 10). A subsurface anticyclonic circulation regime along the trough system was first inferred based on mooring observations in Westwind Trough (Topp & Johnson, 1997) though Budéus et al. (1997) proposed that there was not a one-directional through-flow of deep waters in the trough system. A subsurface boundary current that transports AIW from the continental shelf edge toward 79NG was first proposed by Schaffer et al. (2017) using velocity observations in Norske Trough (Figure 1), and was resolved at sub-annual scales by Münchow et al. (2020). Higher frequency signals on timescales of days to weeks observed in the boundary current in Norske Trough were attributed to Rossby waves, generated by offshore Ekman pumping over the steep topography of the shelf break (Münchow et al., 2020).

Variability at these timescales was also found at the 79NG calving front and below the ice tongue (Lindeman et al., 2020; Schaffer et al., 2020). It was proposed that the Rossby waves on the continental shelf drove oscillations in the AIW isopycnals, which then modulated the inflow strength at the 79NG cavity. This is further supported by results from moored observations at 79NG which demonstrated that the sub-annual heat flux below the glacier is determined by the AIW conditions on the continental shelf (Lindeman et al., 2020; Schaffer et al., 2020; von Albedyll et al., 2021; Wilson & Straneo, 2015). In the results presented here, the interannual variability of the AIW temperature in Norske Trough has a standard deviation that is almost double that of the

seasonal signal (Figure 5c). Therefore, the interannual variability of AIW temperatures, which originates in the WSC, can act to significantly modify the rates of warm AIW inflow to the cavity of the 79NG and ultimately melt rates occurring at the glacier base.

The long-term warming trend present on the NEG continental shelf, observed in both the model output and observations, shows a general increase in AIW temperatures of over 0.6°C from 1970 to 2018 (Figures 3b and 3c). This warming in generally consistent with other estimates on the NEG continental shelf. Schaffer et al. (2016) used an extensive compilation of CTD profiles to determine a robust AIW warming signal of 0.5°C throughout Norske Trough from 1997 to 2016, while numerical simulations found similar AIW warming on the NEG continental shelf of about 0.5°C since the 1970s (Smedsrud et al., 2022). Similar warming of AIW temperatures have also been observed at the calving front and below the cavity of 79NG (Lindeman et al., 2020; Schaffer et al., 2020), suggesting that the AW in the WSC as the advective source of the AIW on the NEG continental shelf controls the thinning and ultimate fate of the NEG outlet glaciers (Khan et al., 2022; Mayer et al., 2018; Mouginot et al., 2015; Wilson & Straneo, 2015).

## 7. Summary

A high-resolution ocean-sea-ice model (FESOM2.1) was used to examine the spatio-temporal distribution and variability of warm AIW on the Northeast Greenland (NEG) continental shelf. It is believed that this warm water drives the submarine melting of the marine-terminating glaciers in NEG, and the ocean conditions on the continental shelf itself determine the melt rate. A bottom-intensified boundary current transports AIW through Norske Trough toward the glaciers as part of an anticyclonic shelf circulation. It was found that the interannual AIW temperature variability on the continental shelf is largely controlled upstream and not on the NEG continental shelf itself. The boundary conditions are set in the WSC, in Eastern Fram Strait, and the AW temperature anomalies are then advected westwards, toward Greenland. As the AIW that arrives on the NEG continental shelf first goes through the recirculation, the behavior of the pathways of RAW also plays a crucial role in controlling its variability. Composite maps show that when the AIW temperature anomalies on the NEG continental shelf are high, the northward transport of AW in the WSC is strengthened, and the AW temperature itself is warmer. The northern and middle RAW branches which are fed by the accelerated WSC are also more pronounced, and more AW reaches and migrates onto the more northern parts of the NEG continental shelf edge. There, the increased volume of warmer AIW enters the shelf circulation regime and is propagated through the trough system.

It was shown that positive AIW temperature anomalies on the NEG continental shelf are connected to an anticyclonic wind anomaly in the Barents Sea and over Svalbard. The anomalous winds drive an anomalous Ekman transport toward the coast of Svalbard. The resultant SSH gradient then enhances the northward flow of AW in the WSC, which is then recirculated westwards, and can drive the RAW pathways to higher latitudes.

The fraction of AW that is recirculated in Fram Strait impacts the heat flux on the NEG continental shelf, which in turn determines the melt rate of the glaciers. It also affects the heat transport toward the Arctic Ocean. Our improved understanding of the controlling mechanisms of AIW variability on the NEG continental shelf provides insight into the behavior of the recirculation pathways of AW in Fram Strait and the role of the WSC in determining the continental shelf conditions. As AW in the Fram Strait and Arctic Ocean are undergoing multi-decadal warming, it may be assumed that this increase in oceanic heat will be directly translated into further increasing AIW temperatures and glacier melt rates. However, the persistent sea-ice decline would suggest the presence of wind anomalies that favor a more southern circulation pathway of AW across Fram Strait (Heukamp et al., 2023) and thus cooler AIW temperatures. An understanding of the transport pathways of that enhanced heat may therefore be key to predicting the fate of not only the marine-terminating glaciers in Northeast Greenland, but also that of the Arctic sea-ice.

## Data Availability Statement

The processed CTD data is from Schaffer et al. (2017), Behrendt et al. (2018), OMG (2020), and from the World Data Center PANGAEA (Kanzow et al., 2017, 2018). The processed data from the mooring array across Fram Strait is available from von Appen et al. (2015) and von Appen (2019). Maps based on the RTopo-2 data set are available from Schaffer et al. (2016). FESOM2.1 model source code can be accessed at

https://github.com/FESOM/fesom2. The model output and settings needed to reproduce the results are provided at https://doi.org/10.5281/zenodo.8320904.

**Acknowledgments**
The authors would like to thank Finn Heukamp for helpful discussions about this study. Wilken-Jon von Appen and two reviewers also provided detailed and constructive feedback that improved the manuscript. The mooring and CTD datasets used in this study were funded by multiple different institutional, national, and European projects, and thanks to all who collected and processed the data. This work was supported in part through grant (A2Green) from the Deutsche Forschungsgemeinschaft (DFG) as part of the Special Priority Program (SPP)-1889 "Regional Sea Level Change and Society" (SeaLevel) (Grant 659641). We gratefully acknowledge the funding by DFG through the Transregional Collaborative Research Centre TRR-172 "ArctiC Amplification: Climate Relevant Atmospheric and SurfaCe Processes, and Feedback Mechanisms (AC)3" (Grant 268020496). CW received funding from the Federal Ministry of Education and Research in Germany (BMBF) through the research program "GROCE2" (FKZ 03F0855A). The authors gratefully acknowledge the computing time granted by the Resource Allocation Board and provided on the supercomputer Lise at NHRZIB as part of the NHR infrastructure. The calculations for this research were conducted with computing resources under the project hbk00087. Open Access funding enabled and organized by Projekt DEAL.

## References

Aagaard, K., Foldvik, A., & Hillman, S. R. (1987). The West Spitsbergen current: Disposition and water mass transformation. *Journal of Geophysical Research*, *92*(C4), 3778–3784. https://doi.org/10.1029/JC092iC04p03778

Bamber, J. L., Tedstone, A. J., King, M. D., Howat, I. M., Enderlin, E. M., van den Broeke, M. R., & Noel, B. (2018). Land ice freshwater budget of the Arctic and North Atlantic oceans: 1. Data, methods, and results. *Journal of Geophysical Research: Oceans*, *123*(3), 1827–1837. https://doi.org/10.1002/2017JC013605

Behrendt, A., Sumata, H., Rabe, B., & Schauer, U. (2018). UDASH—Unified database for arctic and subarctic hydrography. *Earth System Science Data*, *10*(2), 1119–1138. https://doi.org/10.5194/essd-10-1119-2018

Beszczynska-Möller, A., Fahrbach, E., Schauer, U., & Hansen, E. (2012). Variability in Atlantic water temperature and transport at the entrance to the Arctic Ocean, 1997–2010. *ICES Journal of Marine Science*, *69*(5), 852–863. https://doi.org/10.1093/icesjms/fss056

Bourke, R. H., Newton, J. L., Paquette, R. G., & Tunnicliffe, M. D. (1987). Circulation and water masses of the East Greenland shelf. *Journal of Geophysical Research*, *92*(C7), 6729–6740. https://doi.org/10.1029/JC092iC07p06729

Boyd, T. J., & D'Asaro, E. A. (1994). Cooling of the West Spitsbergen current: Wintertime observations West of Svalbard. *Journal of Geophysical Research*, *99*(C11), 22597–22618. https://doi.org/10.1029/94JC01824

Budéus, G., Schneider, W., & Kattner, G. (1997). Distribution and exchange of water masses in the Northeast Water polynya (Greenland Sea). *Journal of Marine Systems*, *10*(1–4), 123–138. https://doi.org/10.1016/S0924-7963(96)00074-7

Chafik, L., Nilsson, J., Skagseth, Ã., & Lundberg, P. (2015). On the flow of Atlantic water and temperature anomalies in the Nordic seas toward the Arctic Ocean. *Journal of Geophysical Research: Oceans*, *120*(12), 7897–7918. https://doi.org/10.1002/2015JC011012

Chatterjee, S., Raj, R. P., Bertino, L., Skagseth, Ã., Ravichandran, M., & Johannessen, O. M. (2018). Role of Greenland Sea gyre circulation on Atlantic water temperature variability in the Fram Strait. *Geophysical Research Letters*, *45*(16), 8399–8406. https://doi.org/10.1029/2018GL079174

Cherian, D. A., & Brink, K. H. (2018). Shelf flows forced by deep-ocean anticyclonic eddies at the shelf break. *Journal of Physical Oceanography*, *48*(5), 1117–1138. https://doi.org/10.1175/JPO-D-17-0237.1

Danilov, S., Sidorenko, D., Wang, Q., & Jung, T. (2017). The Finite-volumE Sea ice–Ocean Model (FESOM2). *Geoscientific Model Development*, *10*(2), 765–789. https://doi.org/10.5194/gmd-10-765-2017

Danilov, S., Wang, Q., Timmermann, R., Iakovlev, N., Sidorenko, D., Kimmritz, M., et al. (2015). Finite-element sea ice model (FESOM), version 2. *Geoscientific Model Development*, *8*(6), 1747–1761. https://doi.org/10.5194/gmd-8-1747-2015

de Steur, L., Hansen, E., Gerdes, R., Karcher, M., Fahrbach, E., & Holfort, J. (2009). Freshwater fluxes in the East Greenland current: A decade of observations. *Geophysical Research Letters*, *36*(23), L23611. https://doi.org/10.1029/2009GL041278

de Steur, L., Hansen, E., Mauritzen, C., Beszczynska-Möller, A., & Fahrbach, E. (2014). Impact of recirculation on the East Greenland current in Fram Strait: Results from moored current meter measurements between 1997 and 2009. *Deep Sea Research Part I: Oceanographic Research Papers*, *92*, 26–40. https://doi.org/10.1016/j.dsr.2014.05.018

Engwirda, D. (2017). JIGSAW-GEO (1.0): Locally orthogonal staggered unstructured grid generation for general circulation modelling on the sphere. *Geoscientific Model Development*, *10*(6), 2117–2140. https://doi.org/10.5194/gmd-10-2117-2017

Gaspar, P., Grégoris, Y., & Lefevre, J.-M. (1990). A simple eddy kinetic energy model for simulations of the oceanic vertical mixing: Tests at station Papa and long-term upper ocean study site. *Journal of Geophysical Research*, *95*(C9), 16179–16193. https://doi.org/10.1029/JC095iC09p16179

Gent, P. R., & Mcwilliams, J. C. (1990). Isopycnal mixing in ocean circulation models. *Journal of Physical Oceanography*, *20*(1), 150–155. https://doi.org/10.1175/1520-0485(1990)020⟨0150:IMIOCM⟩2.0.CO;2

Gjelstrup, C. V. B., Sejr, M. K., de Steur, L., Christiansen, J. S., Granskog, M. A., Koch, B. P., et al. (2022). Vertical redistribution of principle water masses on the Northeast Greenland Shelf. *Nature Communications*, *13*, 1–12. https://doi.org/10.1038/s41467-022-35413-z

Griffies, S. M. (1998). The Gent–McWilliams Skew flux. *Journal of Physical Oceanography*, *28*(5), 831–841. https://doi.org/10.1175/1520-0485(1998)028⟨0831:TGMSF⟩2.0.CO;2

Griffies, S. M., Levy, M., Adcroft, A. J., Danabasoglu, G., Hallberg, R. W., Jacobsen, D. J., et al. (2017). The Community ocean vertical mixing (CVMix) project. *Zenodo*. https://doi.org/10.5281/zenodo.1000801

Hattermann, T., Isachsen, P. E., von Appen, W.-J., Albretsen, J., & Sundfjord, A. (2016). Eddy-driven recirculation of Atlantic water in Fram Strait. *Geophysical Research Letters*, *43*(7), 3406–3414. https://doi.org/10.1002/2016GL068323

Håvik, L., Pickart, R. S., Våge, K., Torres, D., Thurnherr, A. M., Beszczynska-Möller, A., et al. (2017). Evolution of the East Greenland current from Fram Strait to Denmark Strait: Synoptic measurements from summer 2012. *Journal of Geophysical Research: Oceans*, *122*(3), 1974–1994. https://doi.org/10.1002/2016JC012228

Håvik, L., & Våge, K. (2018). Wind-driven coastal upwelling and downwelling in the shelfbreak East Greenland current. *Journal of Geophysical Research: Oceans*, *123*(9), 6106–6115. https://doi.org/10.1029/2018JC014273

Håvik, L., Våge, K., Pickart, R. S., Harden, B., von Appen, W.-J., Jónsson, S., & Østerhus, S. (2017). Structure and variability of the shelfbreak East Greenland current North of Denmark Strait. *Journal of Physical Oceanography*, *47*(10), 2631–2646. https://doi.org/10.1175/JPO-D-17-0062.1

Hellmer, H., & Olbers, D. (1989). A two-dimensional model for the thermohaline circulation under an ice shelf. *Antarctic Science*, *1*(4), 325–336. https://doi.org/10.1017/S0954102089000490

Heukamp, F. O., Kanzow, T., Wang, Q., Wekerle, C., & Gerdes, R. (2023). Impact of cyclonic wind anomalies caused by massive winter sea ice retreat in the Barents Sea on Atlantic water transport towards the Arctic: A model study. *Journal of Geophysical Research: Oceans*, *128*(3), e2022JC019045. https://doi.org/10.1029/2022JC019045

Hofmann, Z., von Appen, W.-J., & Wekerle, C. (2021). Seasonal and mesoscale variability of the two Atlantic water recirculation pathways in Fram Strait. *Journal of Geophysical Research: Oceans*, *126*, 1–18. https://doi.org/10.1029/2020JC017057

Holland, D. M., & Jenkins, A. (1999). Modeling thermodynamic ice–ocean interactions at the base of an ice shelf. *Journal of Physical Oceanography*, *29*(8), 1787–1800. https://doi.org/10.1175/1520-0485(1999)029⟨1787:MTIOIA⟩2.0.CO;2

Holland, D. M., Thomas, R. H., de Young, B., Ribergaard, M. H., & Lyberth, B. (2008). Acceleration of Jakobshavn Isbræ triggered by warm subsurface ocean waters. *Nature Geoscience*, *1*(10), 659–664. https://doi.org/10.1038/ngeo316

Jakobsen, P. K. (2003). Near-surface circulation in the northern North Atlantic as inferred from Lagrangian drifters: Variability from the mesoscale to interannual. *Journal of Geophysical Research*, *108*(C8), 3251. https://doi.org/10.1029/2002JC001554

Kanzow, T., Schaffer, J., & Rohardt, G. (2018). Physical oceanography during POLARSTERN cruise PS109 (ARK-XXXI/4). *PANGAEA*. https://doi.org/10.1594/PANGAEA.885358

Kanzow, T., von Appen, W.-J., Schaffer, J., Köhn, E., Tsubouchi, T., Wilson, N., & Wisotzki, A. (2017). Physical oceanography measured with CTD/Large volume Watersampler-system during POLARSTERN cruise PS100 (ARK-XXX/2). *PANGAEA*. https://doi.org/10.1594/PANGAEA.871025

Khan, S. A., Choi, Y., Morlighem, M., Rignot, E., & Helm, V. (2022). Extensive inland thinning and speed-up of Northeast Greenland ice stream (p. 611). https://doi.org/10.1038/s41586-022-05301-z

Khan, S. A., Kjær, K. H., Bevis, M., Bamber, J. L., Wahr, J., Kjeldsen, K. K., et al. (2014). Sustained mass loss of the northeast Greenland ice sheet triggered by regional warming. *Nature Climate Change*, *4*, 292–299. https://doi.org/10.1038/nclimate2161

Kjeldsen, K. K., Korsgaard, N. J., Bjørk, A. A., Khan, S. A., Box, J. E., Funder, S., et al. (2015). Spatial and temporal distribution of mass loss from the Greenland Ice Sheet since AD 1900. *Nature*, *528*(7582), 396–400. https://doi.org/10.1038/nature16183

Lindeman, M. R., Straneo, F., Wilson, N. J., Toole, J. M., Krishfield, R. A., Beaird, N. L., et al. (2020). Ocean circulation and variability beneath Nioghalvfjerdsbræ (79 North Glacier) ice tongue. *Journal of Geophysical Research: Oceans*, *125*(8), 1–20. https://doi.org/10.1029/2020JC016091

Mankoff, K. D., Fettweis, X., Langen, P. L., Stendel, M., Kjeldsen, K. K., Karlsson, N. B., et al. (2021). Greenland ice sheet mass balance from 1840 through next week. *Earth System Science Data*, *13*(10), 5001–5025. https://doi.org/10.5194/essd-13-5001-2021

Mankoff, K. D., Noël, B., Fettweis, X., Ahlstrøm, A. P., Colgan, W., Kondo, K., et al. (2020). Greenland liquid water discharge from 1958 through 2019. *Earth System Science Data*, *12*(4), 2811–2841. https://doi.org/10.5194/essd-12-2811-2020

Mankoff, K. D., Solgaard, A., Colgan, W., Ahlstrøm, A. P., Khan, S. A., & Fausto, R. S. (2020). Greenland Ice Sheet solid ice discharge from 1986 through March 2020. *Earth System Science Data*, *12*(2), 1367–1383. https://doi.org/10.5194/essd-12-1367-2020

Mayer, C., Schaffer, J., Hattermann, T., Floricioiu, D., Krieger, L., Dodd, P. A., et al. (2018). Large ice loss variability at Nioghalvfjerdsfjorden Glacier, northeast-Greenland. *Nature Communications*, *9*(1), 2768. https://doi.org/10.1038/s41467-018-05180-x

Mouginot, J., Rignot, E., Scheuchl, B., Fenty, I., Khazendar, A., Morlighem, M., et al. (2015). Fast retreat of Zachariae Isstrom, northeast Greenland. *Science*, *350*(6266), 1357–1361. https://doi.org/10.1126/science.aac7111

Muilwijk, M., Ilicak, M., Cornish, S. B., Danilov, S., Gelderloos, R., Gerdes, R., et al. (2019). Arctic Ocean response to Greenland sea wind anomalies in a suite of model simulations. *Journal of Geophysical Research: Oceans*, *124*(8), 6286–6322. https://doi.org/10.1029/2019JC015101

Muilwijk, M., Smedsrud, L. H., Ilicak, M., & Drange, H. (2018). Atlantic water heat transport variability in the 20th Century Arctic Ocean from a global ocean model and observations. *Journal of Geophysical Research: Oceans*, *123*(11), 8159–8179. https://doi.org/10.1029/2018JC014327

Münchow, A., Schaffer, J., & Kanzow, T. (2020). Ocean circulation connecting Fram Strait to glaciers off northeast Greenland: Mean flows, topographic rossby waves, and their forcing. *Journal of Physical Oceanography*, *50*(2), 509–530. https://doi.org/10.1175/JPO-D-19-0085.1

OMG. (2020). OMG. 2020. OMG conductivity temperature depth (CTD) profiles. https://doi.org/10.5067/OMGEV-CTDS1

Polyakov, I. V., Pnyushkov, A. V., Alkire, M. B., Ashik, I. M., Baumann, T. M., Carmack, E. C., et al. (2017). Greater role for Atlantic inflows on sea-ice loss in the Eurasian basin of the Arctic Ocean. *Science*, *356*(6335), 285–291. https://doi.org/10.1126/science.aai8204

Quadfasel, D., Gascard, J.-C., & Koltermann, K.-P. (1987). Large-scale oceanography in Fram Strait during the 1984 marginal ice Zone experiment. *Journal of Geophysical Research*, *92*(C7), 6719–6728. https://doi.org/10.1029/JC092iC07p06719

Redi, M. H. (1982). Oceanic isopycnal mixing by coordinate rotation. *Journal of Physical Oceanography*, *12*(10), 1154–1158.

Richter, M. E., von Appen, W.-J., & Wekerle, C. (2018). Does the East Greenland current exist in the northern Fram Strait? *Ocean Science*, *14*(5), 1147–1165. https://doi.org/10.5194/os-14-1147-2018

Rudels, B. (1987). On the mass balance of the Polar Ocean, with special emphasis on the Fram Strait. *Norsk Polarinstitutt Skrifter*, *188*, 53.

Rudels, B., Björk, G., Nilsson, J., Winsor, P., Lake, I., & Nohr, C. (2005). The interaction between waters from the Arctic Ocean and the Nordic seas north of Fram Strait and along the East Greenland current: Results from the Arctic Ocean-02 Oden expedition. *Journal of Marine Systems*, *55*(1–2), 1–30. https://doi.org/10.1016/j.jmarsys.2004.06.008

Rudels, B., Korhonen, M., Budéus, G., Beszczynska-Möller, A., Schauer, U., Nummelin, A., et al. (2012). The East Greenland current and its impacts on the Nordic seas: Observed trends in the past decade. *ICES Journal of Marine Science*, *69*(5), 841–851. https://doi.org/10.1093/icesjms/fss079

Schaffer, J., Kanzow, T., von Appen, W.-J., von Albedyll, L., Arndt, J. E., & Roberts, D. H. (2020). Bathymetry constrains ocean heat supply to Greenland's largest glacier tongue. *Nature Geoscience*, *13*(3), 227–231. https://doi.org/10.1038/s41561-019-0529-x

Schaffer, J., Timmermann, R., Arndt, J. E., Kristensen, S. S., Mayer, C., Morlighem, M., & Steinhage, D. (2016). A global, high-resolution data set of ice sheet topography, cavity geometry, and ocean bathymetry. *Earth System Science Data*, *8*(2), 543–557. https://doi.org/10.5194/essd-8-543-2016

Schaffer, J., von Appen, W.-J., Dodd, P. A., Hofstede, C., Mayer, C., de Steur, L., & Kanzow, T. (2017). Warm water pathways toward Nioghalvfjerdsfjorden Glacier, northeast Greenland. *Journal of Geophysical Research: Oceans*, *122*(5), 4004–4020. https://doi.org/10.1002/2016JC012462

Schauer, U. (2004). Arctic warming through the Fram Strait: Oceanic heat transport from 3 years of measurements. *Journal of Geophysical Research*, *109*(C6), C06026. https://doi.org/10.1029/2003JC001823

Schauer, U., Beszczynska-Möller, A., Walczowski, W., Fahrbach, E., Piechura, J., & Hansen, E. (2008). Variation of measured heat flow through the Fram Strait between 1997 and 2006. In *Arctic–subarctic ocean fluxes* (pp. 65–85).

Scholz, P., Sidorenko, D., Danilov, S., Wang, Q., Koldunov, N., Sein, D., & Jung, T. (2022). Assessment of the Finite-VolumE Sea ice–Ocean Model (FESOM2.0)—Part 2: Partial bottom cells, embedded sea ice and vertical mixing library CVMix. *Geoscientific Model Development*, *15*(2), 335–363. https://doi.org/10.5194/gmd-15-335-2022

Scholz, P., Sidorenko, D., Gürses, Ö., Danilov, S., Koldunov, N., Wang, Q., et al. (2019). Assessment of the Finite-volumE Sea ice-Ocean Model (FESOM2.0)—Part 1: Description of selected key model elements and comparison to its predecessor version. *Geoscientific Model Development*, *12*(11), 4875–4899. https://doi.org/10.5194/gmd-12-4875-2019

Serreze, M. C., Barrett, A. P., Slater, A. G., Woodgate, R. A., Aagaard, K., Lammers, R. B., et al. (2006). The large-scale freshwater cycle of the Arctic. *Journal of Geophysical Research*, *111*(C11), C11010. https://doi.org/10.1029/2005JC003424

Shepherd, A., Ivins, E. R., Barletta, V. R., Bentley, M. J., Bettadpur, S., Briggs, K. H., et al. (2012). A reconciled estimate of ice-sheet mass balance. *Science*, *338*(6111), 1183–1189. https://doi.org/10.1126/science.1228102

Smedsrud, L. H., Muilwijk, M., Brakstad, A., Madonna, E., Lauvset, S. K., Spensberger, C., et al. (2022). *Nordic seas heat loss, Atlantic inflow, and Arctic sea ice cover over the last century* (Vol. 60). John Wiley and Sons Inc. https://doi.org/10.1029/2020RG000725

Steele, M., Morley, R., & Ermold, W. (2001). PHC: A global ocean hydrography with a high-quality Arctic Ocean. *Journal of Climate*, *14*(9), 2079–2087. https://doi.org/10.1175/1520-0442(2001)014⟨2079:PAGOHW⟩2.0.CO;2

Straneo, F., & Heimbach, P. (2013). North Atlantic warming and the retreat of Greenland's outlet glaciers. *Nature*, *504*(7478), 36–43. https://doi.org/10.1038/nature12854

Sumata, H., de Steur, L., Divine, D. V., Granskog, M. A., & Gerland, S. (2023). Regime shift in Arctic Ocean sea ice thickness. *Nature*, *615*(7952), 443–449. https://doi.org/10.1038/s41586-022-05686-x

Sumata, H., de Steur, L., Gerland, S., Divine, D. V., & Pavlova, O. (2022). Unprecedented decline of Arctic sea ice outflow in 2018. *Nature Communications*, *13*(1), 1747. https://doi.org/10.1038/s41467-022-29470-7

Timmermann, R., Wang, Q., & Hellmer, H. (2012). Ice-shelf basal melting in a global finite-element sea-ice/ice-shelf/ocean model. *Annals of Glaciology*, *53*(60), 303–314. https://doi.org/10.3189/2012AoG60A156

Timmermans, M. L., & Marshall, J. (2020). Understanding Arctic Ocean circulation: A review of ocean dynamics in a changing climate. *Journal of Geophysical Research: Oceans*, *125*(4), e2018JC014378. https://doi.org/10.1029/2018JC014378

Topp, R., & Johnson, M. (1997). Winter intensification and water mass evolution from yearlong current meters in the Northeast Water Polynya. *Journal of Marine Systems*, *10*(1–4), 157–173. https://doi.org/10.1016/S0924-7963(96)00083-8

Tsubouchi, T., von Appen, W.-J., Kanzow, T., & de Steur, L. (2023). Temporal variability of the overturning circulation in the Arctic Ocean and the associated heat and freshwater transports during 2004-2010., *13*, 104–116.

Tsujino, H., Urakawa, S., Nakano, H., Small, R. J., Kim, W. M., Yeager, S. G., et al. (2018). JRA-55 based surface dataset for driving ocean–sea-ice models (JRA55-do). *Ocean Modelling*, *130*, 79–139. https://doi.org/10.1016/j.ocemod.2018.07.002

Tverberg, V., & Nost, O. A. (2009). Eddy overturning across a shelf edge front: Kongsfjorden, West Spitsbergen. *Journal of Geophysical Research*, *114*(C4), 1–15. https://doi.org/10.1029/2008JC005106

van den Broeke, M., Bamber, J., Ettema, J., Rignot, E., Schrama, E., van de Berg, W. J., et al. (2009). Partitioning recent Greenland mass loss. *Science*, *326*(5955), 984–986. https://doi.org/10.1126/science.1178176

von Albedyll, L., Schaffer, J., & Kanzow, T. (2021). Ocean variability at Greenland's largest glacier tongue linked to continental shelf circulation. *Journal of Geophysical Research: Oceans*, *126*, 1–30. https://doi.org/10.1029/2020JC017080

von Appen, W.-J. (2019). Physical oceanography and current meter data (including raw data) from FRAM moorings in the Fram Strait, 2016 - 2018. *PANGAEA*. https://doi.org/10.1594/PANGAEA.904565

von Appen, W.-J., Schauer, U., Cabrillo, R. S., Bauerfeind, E., & Beszczynska-Möller, A. (2015). Physical oceanography and current meter data from mooring and CTD measurements at Fram Strait. *PANGAEA*. https://doi.org/10.1594/PANGAEA.845938

von Appen, W.-J., Schauer, U., Hattermann, T., & Beszczynska-Möller, A. (2016). Seasonal cycle of mesoscale instability of the West Spitsbergen current. *Journal of Physical Oceanography*, *46*(4), 1231–1254. https://doi.org/10.1175/JPO-D-15-0184.1

Wang, Q., Ricker, R., & Mu, L. (2021). Arctic Sea ice decline preconditions events of anomalously low sea ice volume export through Fram Strait in the early 21st century. *Journal of Geophysical Research: Oceans*, *126*(2), e2020JC016607. https://doi.org/10.1029/2020JC016607

Wang, Q., Wekerle, C., Wang, X., Danilov, S., Koldunov, N., Sein, D., et al. (2020). Intensification of the Atlantic water supply to the Arctic Ocean through fram strait induced by Arctic sea ice decline. *Geophysical Research Letters*, *47*(3), e2019GL086682. https://doi.org/10.1029/2019GL086682

Wekerle, C., Hattermann, T., Wang, Q., Crews, L., von Appen, W.-J., & Danilov, S. (2020). Properties and dynamics of mesoscale eddies in Fram Strait from a comparison between two high-resolution ocean-sea ice models. *Ocean Science*, *16*(5), 1225–1246. https://doi.org/10.5194/os-16-1225-2020

Wekerle, C., Wang, Q., von Appen, W.-J., Danilov, S., Schourup-Kristensen, V., & Jung, T. (2017). Eddy-resolving simulation of the Atlantic water circulation in the Fram Strait with focus on the seasonal cycle. *Journal of Geophysical Research: Oceans*, *122*(11), 8385–8405. https://doi.org/10.1002/2017JC012974

Willcox, E. W., Bendtsen, J., Mortensen, J., Mohn, C., Lemes, M., Pedersen, T. J., et al. (2023). An updated view of the water masses on the northeast Greenland Shelf and their link to the Laptev Sea and Lena River. *Journal of Geophysical Research: Oceans*, *128*(4), e2022JC019052. https://doi.org/10.1029/2022JC019052

Wilson, N., & Straneo, F. (2015). Water exchange between the continental shelf and the cavity beneath Nioghalvfjerdsbræ (79 North Glacier). *Geophysical Research Letters*, *42*(18), 7648–7654. https://doi.org/10.1002/2015GL064944

Wilson, N., Straneo, F., & Heimbach, P. (2017). Satellite-derived submarine melt rates and mass balance (2011–2015) for Greenland's largest remaining ice tongues. *The Cryosphere*, *11*(6), 2773–2782. https://doi.org/10.5194/tc-11-2773-2017

Wood, M., Rignot, E., Fenty, I., An, L., Bjørk, A., van den Broeke, M., et al. (2021). Ocean forcing drives glacier retreat in Greenland. *Science Advances*, *7*(1). https://doi.org/10.1126/sciadv.aba7282